

# Chapter 3

## High Strain Rate Studies of Polymer and Hybrid Nanocomposites for Aerospace Application



S. Gurusideswar, R. Velmurugan, and R. Sarathi

### 1 Introduction

Traditionally, polymers have been added with natural or synthetic fillers in order to enhance their mechanical, thermal and electrical properties and also to reduce the cost. They are extensively used in aerospace, automotive, defence and electronics industries. It is proved that the dispersion of nanosized fillers with a larger aspect ratio in polymers leads to dramatic improvement in properties. Among all the potential fillers, clay or layered silicates have been widely used because of their natural abundance, easy availability, high aspect ratio, low cost and environment-friendly nature. Clay/polymer nanocomposites show tremendous enhancement in a wide range of engineering properties and this recent technology can now be applied commercially. The mechanical properties of most of the polymers and its matrix composites are sensitive to strain rates, and in many practical cases, they are subjected to dynamic loadings, which require prior knowledge of dynamic mechanical properties to prevent catastrophic failure during its service. In practical scenarios, the composite structures undergo high-velocity impact loadings (Nurazzi et al., 2021; Suriani et al., 2021). A few examples are collision, crash landing, rigid body impact on a structure, bird impact on jet engine compressor rotating blades, automotive

---

S. Gurusideswar

Department of Aerospace Engineering, SRM Institute of Science and Technology,  
Chennai, India

Department of Aerospace Engineering, Indian Institute of Technology Madras, Chennai, India

R. Velmurugan (✉)

Department of Aerospace Engineering, Indian Institute of Technology Madras, Chennai, India  
e-mail: [ramanv@iitm.ac.in](mailto:ramanv@iitm.ac.in)

R. Sarathi

Department of Electrical Engineering, Indian Institute of Technology Madras, Chennai, India

vehicle components, satellite solar panel, ship hull structures, shock loads, bomb blasts, etc. In order to understand the dynamic behaviour of epoxy, glass/epoxy and its clay nanocomposites, the current research work focuses on the strain rate effects (low and high) of these composites.

Most of the thermoset resins are inherently brittle, which restricts its performance to many structural applications. In general, polymers are being incorporated with micro fillers, such as calcium carbonate, glass beads, mica and talc, in order to enhance their performance. However, it is often reported that the addition of these fillers has certain drawbacks such as an increase in weight, brittleness and opacity (Pavlidou & Papaspyrides, 2008). It is also reported that the properties of those materials can be customized by changing the weight fraction, shape and size of the fillers. A further enhancement in performance can be achieved by adding fillers in the nanometre range, which have a high aspect ratio (Tjong, 2006). The addition of fillers in polymers for which at least one dimension of the dispersed particles is in the nanometre range (<100 nm) is known as nanocomposites. Nanocomposites are considered as one of the classes of nanomaterials, where nanofillers are dispersed in the matrix phase.

Many researchers (Pavlidou & Papaspyrides, 2008; Azeez et al., 2013; Kotal & Bhowmick, 2015; Clifton et al., 2020; Sanusi et al., 2020; Omran et al., 2021; Alsubari et al., 2021; Mohd Nurazzi et al., 2021; Suriani et al., 2021) have devoted themselves to the field of “nanocomposites”, mainly focusing on manufacturing, characterization, fracture mechanism, wear resistance and so on. In actual scenario, polymeric materials and their composites are subjected to dynamic loading and high strain rate deformation in a wide range of aerospace applications. Also, simulation of composite structures under high strain rate deformation requires a clear identification of the strain rate effect on the material behaviour. Hence, high strain rate studies are important, which is not reported in the above-mentioned literature.

Very few literature report the dynamic mechanical responses of this kind of nanocomposites due to the difficulty of high strain rate testing and data interpretation. It is noted that the viscoelastic nature of polymers exhibits significant rate dependence in its stress–strain responses. The effect of the strain rate on the mechanical properties of epoxy nanocomposites was rarely studied, and the data is very limited (Guo & Li, 2007). Chen et al. (2002) modified the split-Hopkinson tension bar (SHTB) to obtain the dynamic stress–strain responses ( $2.5 \times 10^{-3}$ – $1.2 \times 10^3 \text{ s}^{-1}$ ) of epoxy resin and polymethyl methacrylate (PMMA) in compression and tension loadings. They observed that the tensile stress–strain response of both epoxy and PMMA polymer differs significantly from compressive response. Gilat et al. (2007) investigated the mechanical response of two different epoxy resins at different strain rates of  $5 \times 10^{-5}$ , 2, and  $450$ – $700 \text{ s}^{-1}$  in shear and tensile loadings and found that the maximum stress is the same for intermediate and high strain rate testing and lower for low strain rate testing. Evora and Shukla (2003) employed direct ultrasonication technique for fabricating polyester/TiO<sub>2</sub> nanocomposites and observed that the presence of TiO<sub>2</sub> nanoparticles had a significant effect on quasi-static fracture toughness and dynamic modulus and no marked effect on ultimate strength at high strain rate ( $2000 \text{ s}^{-1}$ ). Roland et al. (2007)

studied the effects of strain rates ( $0.06\text{--}573\text{ s}^{-1}$ ) on tensile properties for an elastomeric polyurea using a drop weight test instrument and found an increase in stiffness and failure stress and a decrease in failure strain with increasing strain rate. Guo and Li (2007) studied the quasi-static and dynamic compression behaviour of  $\text{SiO}_2/\text{epoxy}$  nanocomposites at different strain rates ( $10^{-4}\text{--}10^4\text{ s}^{-1}$ ) using desktop split-Hopkinson pressure bar (SHPB) and found that the nanocomposites are sensitive to loading rate and nanoparticle dispersion. Zebarjad and Sajjadi (2008) investigated the effect of nano-sized calcium carbonate and strain rate ( $0.1\text{ s}^{-1}$ ) on the tensile properties of high-density polyethylene (HDPE) and concluded that strain-rate sensitivity of HDPE decreased with the addition of nanofillers. Xiao (2008) carried out the dynamic tensile test using a servo-hydraulic machine on different polymers. Fu et al. (2009) performed dynamic tensile tests ( $1750\text{ s}^{-1}$ ) on polycarbonate using a split-Hopkinson tension bar (SHTB) system and found that the tensile behaviour of polycarbonate is dependent on the strain rate. Raisch and Möglinger (2010) discussed the modification of the clamps of a servo-hydraulic tensile testing machine to achieve a strain rate of  $670\text{ s}^{-1}$  and observed that both tensile modulus and tensile yield stress increase logarithmically with the strain rate. Cao et al. (2010) studied the effect of strain rate on the tensile response of polycarbonate over a wide range of strain rates ( $0.001\text{ s}^{-1}\text{--}1700\text{ s}^{-1}$ ) using the servo-hydraulic machine, a moderate strain testing apparatus and split Hopkinson tension bar and observed that the material is highly sensitive to strain rate. They also proposed a viscoelastic constitutive model to describe the stress–strain response of polycarbonate over a wide range of strain rates. All the above studies are carried out on different polymers at high strain rates. The motivation of this work is to study the effect of medium strain rates on epoxy/clay nanocomposites, which is not reported in the literature.

Composites are generally rate sensitive. Many researchers reported that glass/epoxy composites have shown an increase in tensile modulus and strength as strain rate increases (Lifshitz & Rotem, 1972; Armenàkas & Sciammarella, 1973; Davies & Magee, 1975). Several techniques were developed to study the rate sensitivity of composites for a wide range of strain rates such as conventional loading frame, servo-hydraulic testing machine, drop mass setup and SHPB technique. Daniel et al. (1981) developed a method called expanding ring technique for testing and characterizing graphite/epoxy composites at strain rates in the regime of  $100\text{--}500\text{ s}^{-1}$ . Kawata et al. (1981) introduced SHPB technique for tensile testing of composites at high strain rates. Harding and Welsh (1983) and Staab and Gilat (1995) modified the SHPB for dynamic testing of composites. Hayes and Adams (1982) studied the strain rate effects of glass/epoxy and graphite/epoxy composites using a pendulum impactor. Hamouda and Hashmi (1998) discussed several techniques for obtaining the mechanical behaviour of composite materials under impact loading at high strain rates. Jacob et al. (2004) reviewed the strain rate dependence of mechanical properties of composite materials. Majzoobi et al. (2007) achieved strain rates up to  $10,000\text{ s}^{-1}$  using flying wedge apparatus for testing composites.

In literature, many studies employed SHPB apparatus for high strain rates, which works in a high strain rate range and it is expensive. It was found that the

experimental techniques to determine tensile properties at medium range strain rates of  $1\text{--}100\text{ s}^{-1}$  are not well established (Xiao, 2008). The conventional servo-hydraulic machine is restricted to lower strain rates ( $<10\text{ s}^{-1}$ ), due to its inertial effects of the load cell and grips. The drop mass test setup is inexpensive and it can accommodate different specimen geometries and strain rates. Lifshitz (1976) studied the tensile strength under dynamic loading of glass/epoxy composites using an instrumented drop weight apparatus, and failure stresses were found to be 20–30% higher than the static values; however, failure strain and modulus were the same for static and dynamic loadings. Groves et al. (1993) studied the high strain rate effects between  $0.0001\text{ s}^{-1}$  and  $2660\text{ s}^{-1}$  for carbon fibre-reinforced polymer composites and found an unexpected exponential-like increase in strength and modulus beyond strain rates of  $10\text{ s}^{-1}$  due to high-intensity stress waves. They also observed changes in the fracture propagation pattern. The setup is made for compression loading and limited to  $10\text{ s}^{-1}$  due to high-intensity stress waves. In the current work, a drop mass tower with specimen fixture is designed and fabricated for tensile loading and can accommodate strain rates up to  $500\text{ s}^{-1}$ . Barré et al. (1996) studied the dynamic response ( $10^{-1}\text{--}10^1\text{ s}^{-1}$ ) of glass phenolic/polyester composites and found that the tensile modulus and strength tend to increase with strain rate. It was reported that the use of falling weight tup leads to vibration waves, which are superimposed on the load curve. Okoli (2001) carried out tensile, shear and bending tests to measure energy absorbed to failure of a material by instrumented impact tester on glass/epoxy composites at increasing strain rates. He found an increase in tensile, shear and flexural energy of 17%, 5.9% and 8.5%, respectively, for the strain rates from  $0.0106\text{ s}^{-1}$  to  $2.72\text{ s}^{-1}$  per decade of increase in the log of strain rate. The instrumented impact tester is restricted to a velocity of 4 m/s for flexural impact. The strain rate effects on tensile properties in the range of low strain rates ( $0.00017\text{--}0.00830\text{ s}^{-1}$ ) and medium strain rates ( $0.1\text{--}20\text{ s}^{-1}$ ) were carried out using a low-speed tensile testing machine and servo-hydraulic machine. Pardo et al. (2002) investigated the tensile behaviour of glass/polyester composites at different strain rates using the hydraulic testing machine and found an increase in tensile properties. A maximum of 20 m/s (approximately  $100\text{ s}^{-1}$ ) was reported. Shokrieh and Omidi (2009) investigated the dynamic response of glass/epoxy composites at different strain rates using a servo-hydraulic testing machine equipped with a special jig and fixture. They found an increase of 52% in tensile strength, 12% in tensile modulus, 10% in failure strain and 53% in absorbed failure energy as the strain rate increased from  $0.001$  to  $100\text{ s}^{-1}$ . Though servo-hydraulic testing apparatus with a jig and fixture can accommodate medium strain rates, it restricts the strain rate to  $160\text{ s}^{-1}$  and it is also expensive. Also, it is reported that servo-hydraulic equipment suffers from system ringing (noise) effects. The present study provides a cost-effective solution to tensile testing and can accommodate a wide range of intermediate strain rates. Brown et al. (2010) studied the effects of strain rate ( $10^{-3}\text{--}10^2\text{ s}^{-1}$ ) on the tensile, compression and shear properties of glass/polypropylene composites using drop weight tower and found an increase in tension and compression properties, but a decrease in shear properties with increasing strain rate. The modified instrumental falling weight drop tower using a specially designed fixture was

employed to get an intermediate strain rate of  $70 \text{ s}^{-1}$  on dynamic tensile study of glass/polypropylene composites. The current study focuses on dynamic tensile studies on epoxy and glass/epoxy composites with nanofillers, which is required for aircraft and automobile structural applications. Li and Liu (2015) studied the compressive and tensile behaviour of carbon composites using drop weight impact tester with large impacting mass and achieved constant strain rate by employing a shaper material. An affordable testing technique utilizing drop weight impact tester was proposed for characterizing carbon composites at low strain rates. Perogamvros et al. (2016) employed a modified drop tower to achieve medium strain rates ( $1\text{--}200 \text{ s}^{-1}$ ) and validated the experimental results using an explicit finite element code. In recent times, digital image correlation (DIC) technique has been widely accepted and employed in the field of experimental mechanics for the estimation of strain fields on composite surfaces, and the Young's modulus can be calculated from the strain data (Pan, 2018; Janeliukstis & Chen, 2021). Powell et al. (2017) studied the dynamic response ( $0.0001\text{--}200 \text{ s}^{-1}$ ) of unidirectional and woven carbon fibre-reinforced composites using standard uniaxial frame and an intermediate-to-high-speed testing system with 3D digital image correlation system. Elmahdy and Verleysen (2019) investigated the strain rate sensitivity ( $0.003\text{--}645 \text{ s}^{-1}$ ) of woven basalt and glass epoxy composites in tension using split-Hopkinson pressure tension bar and high-speed stereo digital image correlation technique. They observed that both basalt and glass composites show an increase in tensile properties in comparison with quasi-static loading. Naresh et al. (2020) investigated the strain rate dependence of glass and carbon fibre-reinforced polymer (FRP) composites for different stacking sequences using drop mass setup and digital image correlation technique. They observed an increment in tensile strength and modulus and a decrement in percentage of failure strain for both glass and carbon composites from quasi-static loading to a strain rate of  $542 \text{ s}^{-1}$ . They also carried out scanning electron microscopy (SEM) fractography on fractured specimens under the modes of failure at high strain rates. Kim et al. (2021) employed digital image correlation method to quantify the fracture characteristics for polypropylene composites. Weng et al. (2021) studied the shear properties of carbon fibre-reinforced composites under dynamic loading using a high-speed tensile testing system and digital image correlation technique. They also investigated different modes of shear failure for composite specimen under various strain rates.

From the comprehensive summary of published investigations, it is noted that studies on intermediate strain rate regime are rarely reported. It is suggested that the drop tower apparatus with digital image correlation (DIC) technique optical devices is suitable for medium strain rate tensile testing. Hence, in this work an attempt is made to study the effect of strain rates from quasi-static to several hundred per second on the tensile properties of epoxy/clay and glass/epoxy/clay nanocomposites with the application of drop mass system and non-contact DIC technique. The purpose is to improve the performance of polymer and its composites by adding nanoclay as a filler material in high strain rate applications.

## 2 Materials and Methods

### 2.1 Materials

A medium viscous unmodified liquid diglycidylether of bisphenol A (DGEBA) epoxy resin was used for the current work, and the commercial name of the resin is Araldite® LY 556. A low viscous unmodified aliphatic-type triethylenetetramine (TETA) was used as a curing agent and the commercial name of the curing agent is Aradur® HY 951. Both the resin and the curing agent were procured from Huntsman Advanced Materials (Belgium). It is advisable to mix the epoxy and the curing agent in a gentle manner to achieve a homogeneous solution and also to avoid air bubbles during curing. E-glass-type fibre of 610 gsm with woven-roving mat (WRM) architecture was procured from M/s. Sakthi Fibres (India) and used as the primary reinforcement for the fabrication of composites. Modified montmorillonite clay (GARAMITE®-1958) was procured from BYK-Chemie GmbH, Germany (formerly Rockwood Additives), and used as a secondary reinforcement for the fabrication of nanocomposites.

### 2.2 Specimen Preparation

Clay levels of 1.5, 3.0 and 5.0 wt% were chosen to fabricate epoxy/clay nanocomposites. The required amount of clay was first preheated at 50 °C for 2 h to avoid agglomeration due to moisture content, and subsequently the epoxy was preheated at 50 °C for 2 h to reduce the viscosity. The primary dispersion was carried out through mechanical stirring technique and the secondary dispersion was carried out using an ultrasonicator for 10 min. The required amount of curing agent (TETA) was then added to the epoxy/clay mixture and mixed properly to prevent air bubbles, as the epoxy/clay mixture and curing agent were at different viscosities. The epoxy mixture was kept in a vacuum oven at 50 °C for 5 min to remove air voids. A glass mould of dimension 300 × 300 mm was used. Rubber beadings were used to maintain a 3 mm constant thickness all around the mould plates and the wax was used as a releasing agent. The solution was poured into the mould and left for curing at room temperature for 24 h.

Glass/epoxy nanocomposites with clay levels of 1.5, 3.0 and 5.0 wt% were fabricated using hand lay-up technique followed by compression moulding technique. A thin layer of epoxy/organoclay mixture was coated with a brush on an aluminium plate. Then the epoxy/organoclay mixture was impregnated into the WRM glass fibre with the assistance of hand roller to ensure uniform wetting of fibres. The laminates were cured at room temperature and kept in the compression moulding equipment for complete curing.

### 2.3 Testing Techniques

In general, six different types of testing systems are employed to study the strain rate effects of a material. They are as follows:

1. Conventional screw drive load frame ( $<0.1 \text{ s}^{-1}$ )
2. Servo-hydraulic system ( $0.1\text{--}100 \text{ s}^{-1}$ )
3. Drop mass test setup ( $100\text{--}1000 \text{ s}^{-1}$ )
4. Split-Hopkinson pressure bar ( $100\text{--}10^4 \text{ s}^{-1}$ )
5. Expanded ring ( $10^4 \text{ s}^{-1}$ )
6. Flyer plate ( $>10^5 \text{ s}^{-1}$ )

The SHPB apparatus can be employed for high strain rate testing in the region of  $100\text{--}10,000 \text{ s}^{-1}$ . However, it cannot be used in the medium strain rate range ( $1\text{--}100 \text{ s}^{-1}$ ). Servo-hydraulic machines can cover medium strain rates; however, they are not affordable due to its high cost and also it may lead to a system ringing phenomenon. In order to overcome these issues, a drop mass test apparatus is chosen to cover the medium strain rate range for the current work. The drop mass test setup comprises a drop mass tower, specimen fixture, load sensor and data acquisition system (Fig. 3.1).

The guide rods, made up of induction-hardened chrome alloy (CK 45) with a tensile strength of 630 MPa, are used to guide the elevator or impactor unit. The impactor unit, which holds the electromagnet and drop mass, has a linear bearing assembly to enable smooth sliding motion along the two guide rods. The entire drop mass unit can be lifted by an electric motor to a required height. The drop tower is designed for low energy and low-velocity applications, and it can be used to achieve a maximum velocity of 8.5 m/s using 25 kg drop mass, which is computed from where the mass can be dropped. Figure 3.2 shows a typical photograph of specimen fixture. It has two grips, where the specimen is clamped at each end between steel grips. The top grip is directly bolted through the load cell to the fixed carriage. A moving carriage is supported by the lower grip and is guided by three steel rods. The drop tower striker imparts a load on the moving carriage which loads the specimen in tension through the lower grip as it travels downward. To get reliable stress data, an integrated circuit piezoelectric (ICP)-type load sensor is employed to acquire load data at the high-speed environment. It is noted that quartz-type load sensors are recommended for dynamic force applications. However, it cannot be used for static applications. A maximum load of 2224 N can be achieved with the given load sensor.

### 2.4 High-Speed Digital Image Correlation (DIC) Technique

DIC is a non-interferometric optical technique and it is considered as a powerful and flexible tool to get reliable strain data. It is based on digital image processing and numerical computing and it was first developed by a group of researchers at the University of South Carolina in the 1980s. In literature (Pan et al., 2009), digital

**Fig. 3.1** Photograph of drop mass tower with specimen fixture (Gurusideswar et al., 2016), copyright 2021. Reproduced with permission from Elsevier Ltd.

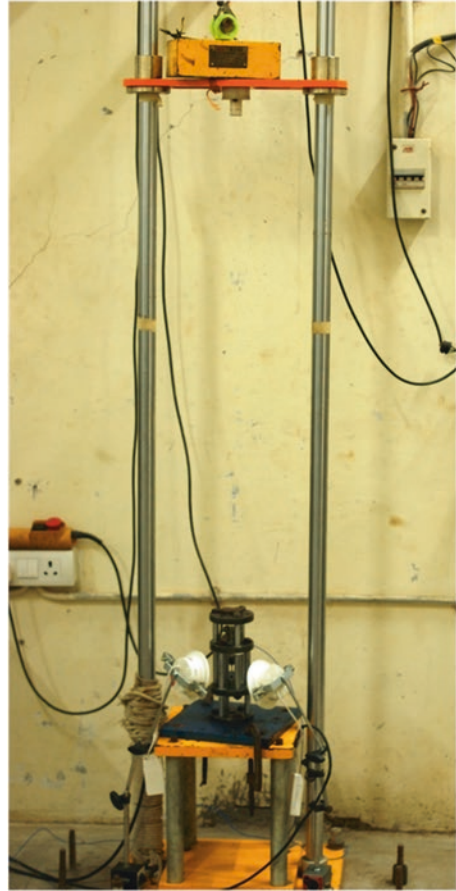
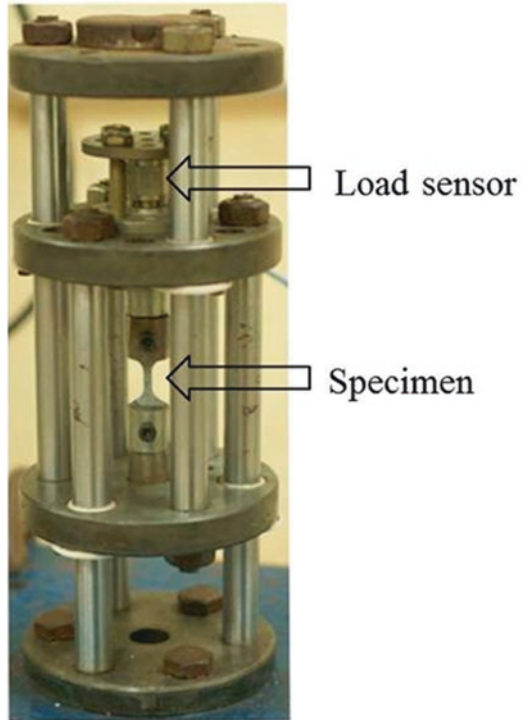


image correlation technique is denoted using different names such as non-contact strain measurement technique, digital speckle correlation method (DSCM), computer-aided speckle interferometry (CASI), electronic speckle photography (ESP) and texture correlation. The basic principle of 2D DIC for the measurement of displacement (strain) involves tracking the movement of points between the two recorded images before and after loading. To achieve this, a virtual grid of subsets of a selected size and shape consisting of pixel grey value distributions is superimposed on the artificially sprayed surface pattern. The purpose of choosing a subset rather than a pixel is to have a wider range of grey-level intensities, which helps to distinguish it from other subsets and to identify it in a unique manner. The processing involves calculation of the average greyscale intensity over the subset of the reference image and deformed image (after loading) and correlating them. In general, the 2D DIC method comprises the following principles:

1. Preparation of specimen (speckle pattern)
2. Recording the images of specimen before and during loading till failure



**Fig. 3.2** Photograph of in-house designed specimen fixture assembly (Gurusideswar et al., 2017), copyright 2021. Reproduced with permission from Elsevier Ltd.



### 3. Post-processing the recorded images using a computer program (image correlation algorithm)

It is noted that the strain measurement accuracy of 2D DIC relies more on the quality of imaging, perfection of loading systems and the selection of post-processing parameters (Pan et al., 2009). From trial runs, the following DIC parameters were optimized and chosen for high strain rate experiments to get accurate and reliable data using the 2D DIC technique:

1. Guarantee parallelism between the CCD camera and the specimen surface
2. 12 W concealed LED lamps
3. 50 mm focal length lens
4. 15 cm distance between the camera and the specimen surface
5. Manual speckle pattern using pen marker to obtain high contrast
6.  $128 \times 128$  pixels to achieve 100,000 fps
7. 19–25 subset size range

In this work, a Phantom® V611 camera was employed to capture images at a high speed. It has a widescreen  $1280 \times 800$  CMOS sensor, which enables it to capture moving targets. A maximum of 6242 frames per second can be achieved at its full resolution, whereas a maximum of 680,000 fps can be achieved at a reduced resolution ( $128 \times 8$  pixels) and also it is possible to achieve 1,000,000 fps using the ‘fast option’.

### 3 Results and Discussion

#### 3.1 High Strain Rate Sensitivity of Epoxy/Clay Nanocomposites

Tensile studies were carried out on the drop mass tower from heights of 0.5, 0.75 and 1 m, producing theoretical strain rates of 315, 385 and 445  $s^{-1}$ , respectively. A drop mass of 0.5 kg was used. Figure 3.3 shows the variation of nominal strain rate versus drop mass height. The actual strain rate can be determined from strain histories, such as the one shown in Fig. 3.4. It is observed that the initial part of the strain–time curve is not truly indicative of the effective strain rate experienced by the specimen, and hence, the actual strain rates were thus determined from the gradient of the strain–time curves (Hsiao & Daniel, 1998; Brown et al., 2010). The averages of actual strain rates during the experiments at heights of 0.5, 0.75 and 1 m (3.1, 3.8 and 4.4  $ms^{-1}$ ) were 25, 41 and 53  $s^{-1}$ , respectively. However, the actual strain rates are used in practice for the purpose of analysis. A significant increase in strain rate at about 75  $\mu s$  could be due to local failure as the duration of impact is very short. An average decrease in strain to failure of 12%, 20% and 27% at 315, 385 and 415  $s^{-1}$ , respectively, is observed for epoxy/clay nanocomposites with respect to quasi-static loading.

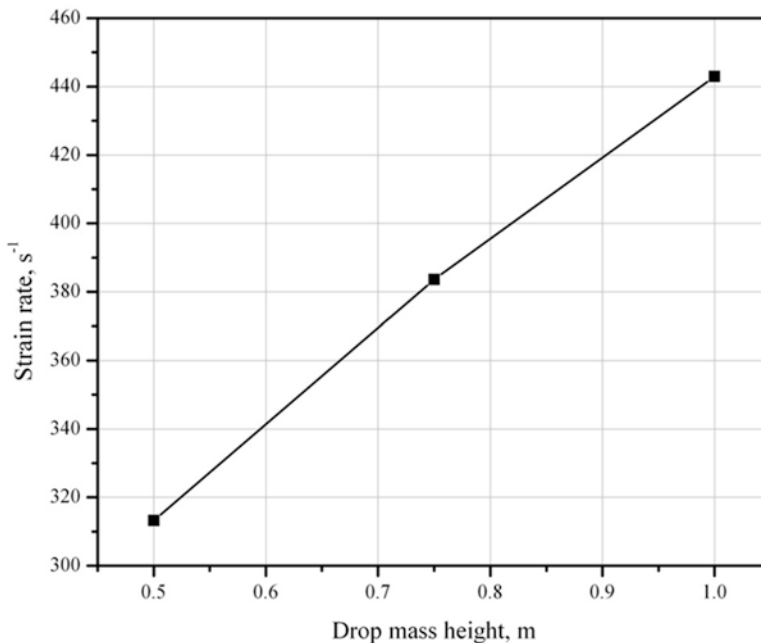
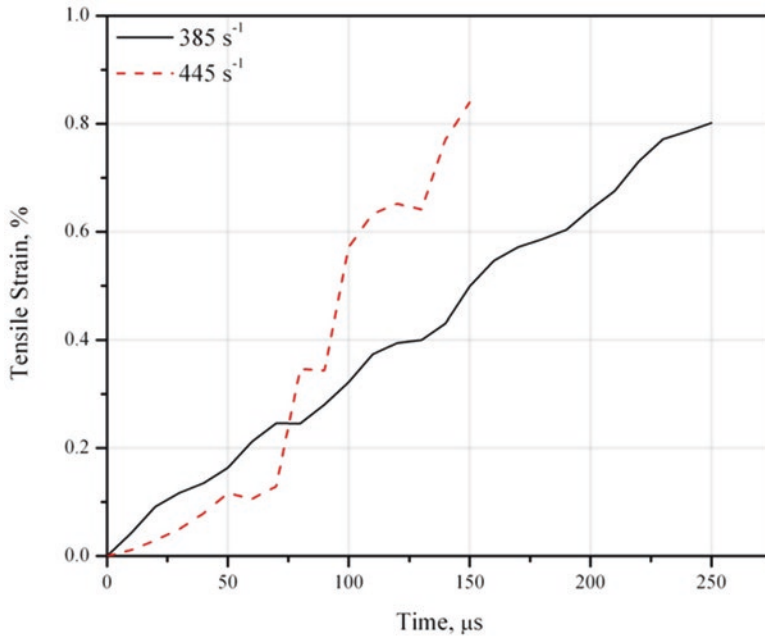


Fig. 3.3 Variation of strain rate versus drop mass height (Gurusideswar et al., 2017), copyright 2021. Reproduced with permission from Elsevier Ltd.



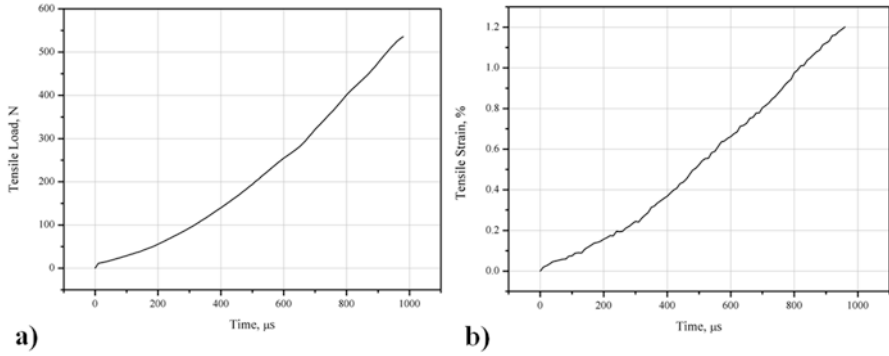
**Fig. 3.4** Strain histories of 3.0 wt% clay/epoxy nanocomposites at strain rates of  $385 \text{ s}^{-1}$  and  $445 \text{ s}^{-1}$  (Gurusideswar et al., 2016), copyright 2021. Reproduced with permission from Elsevier Ltd.

Figure 3.5a and b shows load and strain histories for 1.5 wt% clay nanocomposites at dynamic loading ( $385 \text{ s}^{-1}$ ). The specimen failed at 550 N and the corresponding strain is 1.2% at a drop mass height of 0.75 m, which corresponds to the strain rate of  $385 \text{ s}^{-1}$ .

Figure 3.6a shows stress–strain responses for 1.5 wt% clay nanocomposites at quasi-static and dynamic loadings. At 0.75 m drop mass height corresponding to the strain rate of  $385 \text{ s}^{-1}$ , the stress–strain behaviour is different from quasi-static results. It showed increasing slope and strength with the increase of strain rate. Similar observations are shown in Fig. 3.6b, for the stress–strain behaviour of 3.0 wt% clay nanocomposites at a strain rate of  $445 \text{ s}^{-1}$  relative to quasi-static loading.

Gilat et al. (2007) reported that the strain rate effects could be explained by the shape of stress–strain curves. At high strain rates, deformation during the test involves only short-range intermolecular interactions between polymer chains without appreciable change in the intramolecular configuration (shape) of the large polymer chains (due to the short duration of testing). At lower strain rates, molecular motions are fast enough to allow changes in the intramolecular configuration during the test.

Figure 3.7 shows the strain contour plots of 3.0 wt% clay/epoxy nanocomposites at a strain rate of  $315 \text{ s}^{-1}$  at different time steps. The longitudinal strain ( $\epsilon_{yy}$ ) distribution at  $t_0 + 130 \mu\text{s}$  corresponding to a load value of 84 N is shown in Fig. 3.7a.



**Fig. 3.5** (a) Load and (b) strain histories of 1.5 wt% clay/epoxy nanocomposites at a strain rate of  $385 \text{ s}^{-1}$

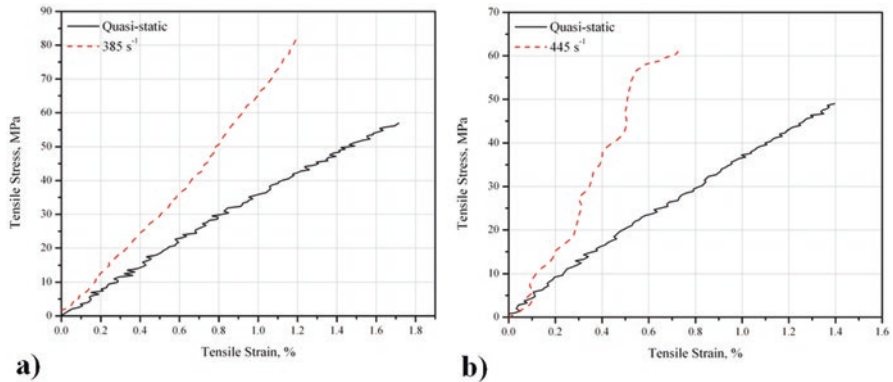


**Fig. 3.6** Stress-strain responses of (a) 1.5 wt% and (b) 3.0 wt% clay/epoxy nanocomposites (Gurusideswar et al., 2016), copyright 2021. Reproduced with permission from Elsevier Ltd.

Similarly, Fig. 3.7b shows strain distribution at  $t_0 + 330 \mu\text{s}$  corresponding to a load value of 327 N. The maximum strain value of 2.36% at  $t_0 + 530 \mu\text{s}$  (467 N) is observed in Fig. 3.7c just before the fracture. Figure 3.7d shows the typical brittle fracture of nanocomposite specimen at  $t_0 + 560 \mu\text{s}$ . The variation in strain could be due to the non-uniform clay distribution and need not be because of bending load. This could be validated from the strain contour plot of glass/epoxy composites (Fig. 3.17), in which the strain is uniform across the specimen width.

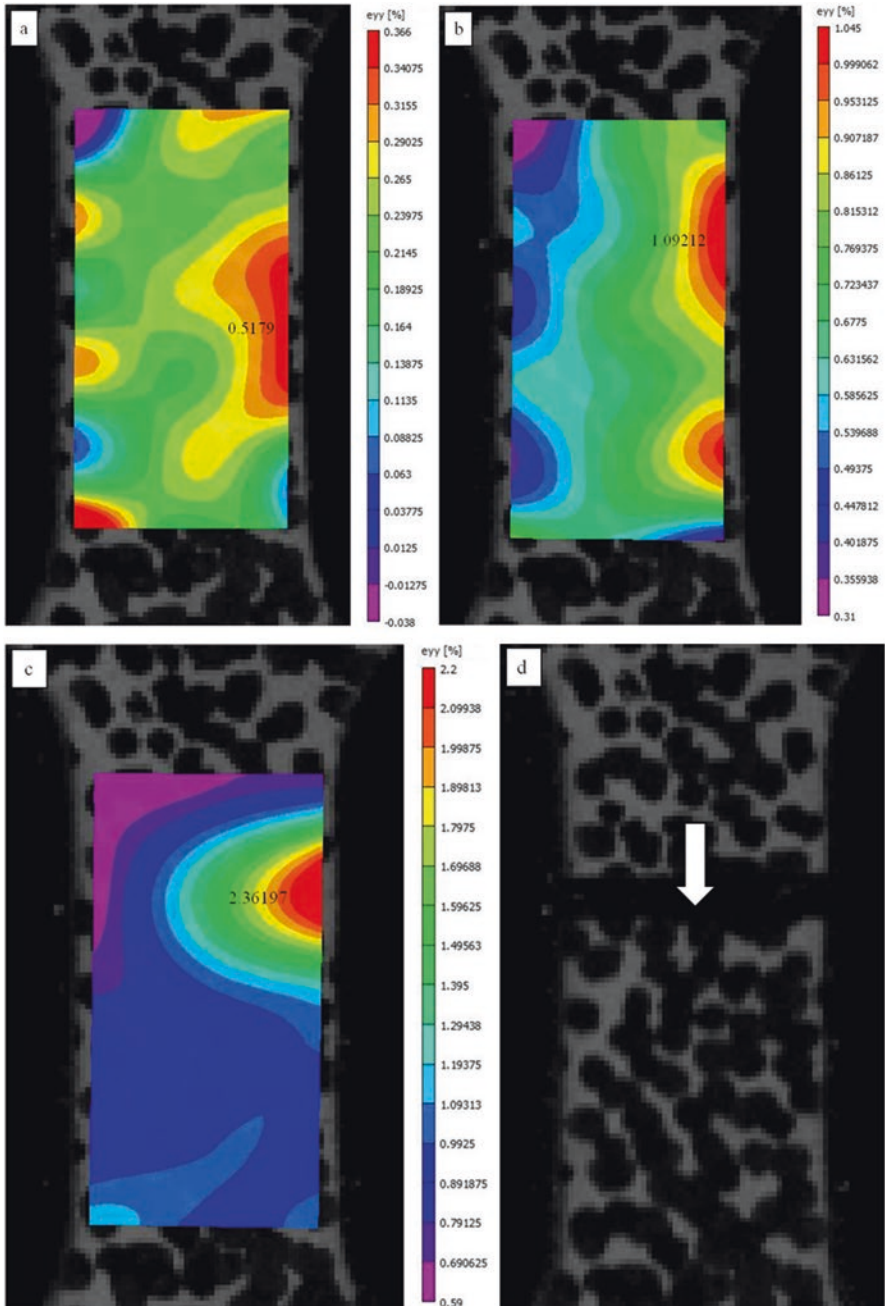


**Fig. 3.7** Strain contour plots of 3.0 wt% clay/epoxy nanocomposites at a strain rate of  $315 \text{ s}^{-1}$  (a)  $t_0 + 130 \mu\text{s}$ , (b)  $t_0 + 330 \mu\text{s}$ , (c)  $t_0 + 530 \mu\text{s}$  and (d)  $t_0 + 560 \mu\text{s}$  (Gurusideswar et al., 2016), copyright 2021. Reproduced with permission from Elsevier Ltd.

### 3.2 Effect of High Strain Rate on Tensile Properties of Epoxy

Figure 3.8 illustrates the effect of strain rate on the tensile modulus on a logarithmic scale. The elastic modulus is calculated by considering the initial slope of the strain–strain response of the material. The VIC 2D software gives the average strain values along the chosen gauge area. The tensile modulus (3.54 GPa) significantly increases up to 77% (6.25 GPa) at the highest strain rate for the neat epoxy system. The same trend is followed for epoxy/clay nanocomposites. An increase of 90%, 83% and 89% in tensile modulus is observed from quasi-static to the highest strain rate of  $445 \text{ s}^{-1}$  (1 m drop mass height) for 1.5 wt%, 3.0 wt% and 5.0 wt% of clay loadings, respectively. The maximum increase (90%) in modulus is observed for 1.5 wt% clay loading at the strain rate of  $445 \text{ s}^{-1}$ .

The tensile modulus and tensile strength are quite sensitive to high strain rates. Figure 3.9 illustrates the effect of strain rate on the tensile strength on a logarithmic scale. The tensile strength (39 MPa) of neat epoxy follows a similar trend, just like the tensile modulus, with an increase of 41% (55 MPa). Buckley et al. (2001) performed tensile tests on three different thermosetting resins and found an increase in modulus of 62%, a marginal increase in maximum stress of 11% and a reduction in failure strain of 41% with increasing strain rate ( $2000 \text{ s}^{-1}$ ) for unmodified diglycidylether of bisphenol A (DGEBA) epoxy resin.

The tensile modulus, strength and failure strain at various strain rates are presented in Table 3.1 for the neat epoxy system, 1.5, 3.0 and 5.0 wt% clay loading, respectively. The increase in tensile modulus and strength is commonly described by the viscoelastic nature of the polymeric matrix (Buckley et al., 2001; Shokrieh & Omid, 2009), i.e. stiffening with increased rate of loading. An increase of 50%, 45% and 25% in tensile strength is observed from quasi-static loading to the highest strain rate of  $445 \text{ s}^{-1}$  (1 m drop mass height) for 1.5, 3.0 and 5.0 wt% clay loadings, respectively, in contrast to quasi-static strain rate. The maximum increase of 50% in

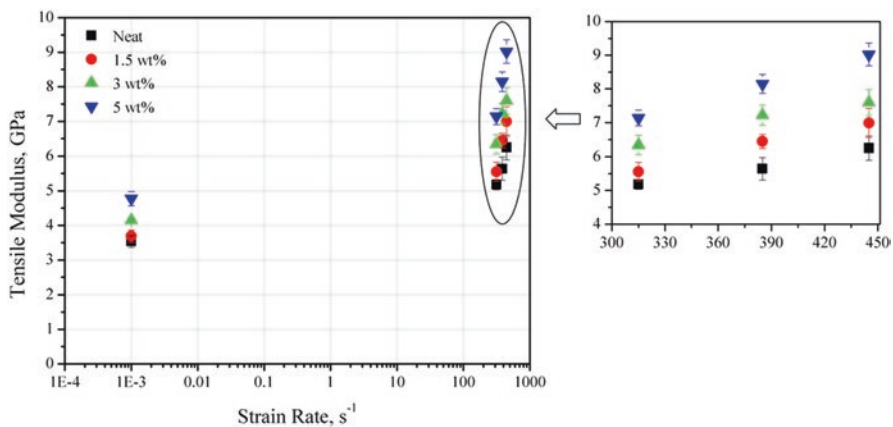


**Fig. 3.8** Effect of high strain rate on tensile modulus of epoxy and its clay nanocomposites

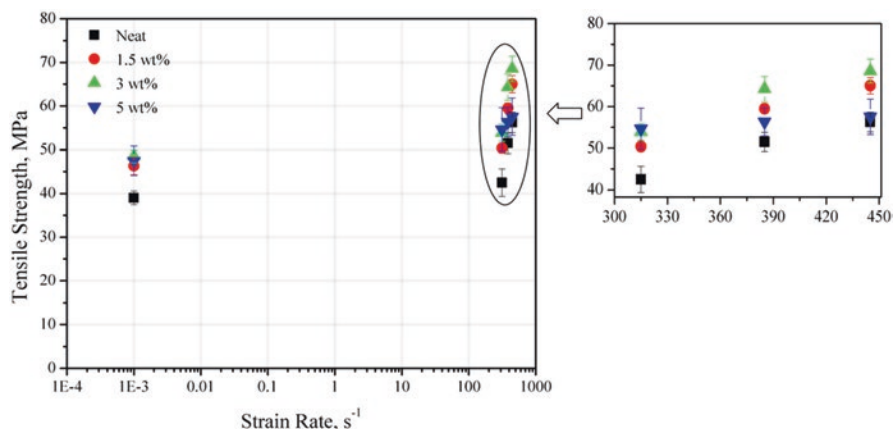


**Fig. 3.9** Effect of high strain rate on tensile strength of epoxy and its clay nanocomposites

**Table 3.1** Effect of high strain rate on tensile properties of epoxy and its clay nanocomposites

Clay content wt%	Drop mass height m	Strain rate $s^{-1}$	Tensile modulus GPa	Tensile strength MPa	Tensile strain %
Neat	Quasi-static	0.001	$3.54 \pm 0.16$	$39 \pm 1.56$	$1.039 \pm 0.014$
	0.5	315	$5.18 \pm 0.15$	$42.5 \pm 3.15$	$0.974 \pm 0.008$
	0.75	385	$5.64 \pm 0.33$	$51.47 \pm 2.32$	$0.928 \pm 0.009$
	1	445	$6.25 \pm 0.35$	$56.24 \pm 2.32$	$0.852 \pm 0.021$
1.5	Quasi-static	0.001	$3.69 \pm 0.18$	$46.3 \pm 1.99$	$1.2 \pm 0.056$
	0.5	315	$5.56 \pm 0.27$	$50.38 \pm 1.1$	$1.031 \pm 0.018$
	0.75	385	$6.45 \pm 0.21$	$65.86 \pm 1.18$	$0.977 \pm 0.022$
	1	445	$7 \pm 0.43$	$69.36 \pm 1.97$	$0.903 \pm 0.016$
3	Quasi-static	0.001	$4.15 \pm 0.07$	$48.5 \pm 1.41$	$1.396 \pm 0.038$
	0.5	315	$6.34 \pm 0.28$	$53.88 \pm 1.97$	$1.264 \pm 0.017$
	0.75	385	$7.22 \pm 0.31$	$66.79 \pm 3.03$	$1.035 \pm 0.004$
	1	445	$7.6 \pm 0.39$	$70.54 \pm 2.89$	$0.95 \pm 0.056$
5	Quasi-static	0.001	$4.77 \pm 0.21$	$47.5 \pm 3.37$	$1.25 \pm 0.059$
	0.5	315	$7.14 \pm 0.23$	$54.64 \pm 4.98$	$0.986 \pm 0.061$
	0.75	385	$8.15 \pm 0.28$	$56.33 \pm 3.36$	$0.926 \pm 0.019$
	1	445	$9.02 \pm 0.34$	$59.53 \pm 4.27$	$0.85 \pm 0.052$

strength is observed for 1.5 wt% clay loading at the strain rate of  $445 s^{-1}$ . From the results, it is found that the tensile modulus of epoxy/clay nanocomposites is more sensitive to strain rates compared to tensile strength. An average of 27% decrease in failure strain is found as strain rate increases for epoxy/clay nanocomposites.

### 3.2.1 Effect of Clay on Tensile Properties of Epoxy

The stress–strain responses (Fig. 3.10) of epoxy and its clay nanocomposite at a strain rate of  $385\text{ s}^{-1}$  reveal that addition of clay leads to brittle failure.

The high specific surface area (of the order of  $800\text{ m}^2/\text{g}$ ) of nanoclay shows dramatic improvements in modulus even at a low content in an epoxy matrix. It is found that the tensile modulus of the clay nanocomposites increases monotonically with increasing clay content. In general, the improvement in elastic modulus is ascribed to the good dispersion of nanosized clay particles and good interfacial adhesion between the particles and the epoxy matrix so that the mobility of polymer chains is restricted under loading (Yasmin et al., 2003; Velmurugan & Mohan, 2004; Wang et al., 2006; Guo & Li, 2007; Zainuddin et al., 2010). From Fig. 3.11, an increment of 35% in tensile modulus is achieved with the addition of 5.0 wt% of clay in epoxy at quasi-static loading. At the highest strain rate ( $445\text{ s}^{-1}$ ), 45% increase in tensile modulus is observed with the addition of 5.0 wt% of clay in epoxy.

Figure 3.12 shows the percentage variation in tensile modulus due to the addition of clay in epoxy at quasi-static and dynamic loadings. 5.0 wt% clay/epoxy samples show maximum improvement in tensile modulus at all strain rates. The combined effect of high strain rate ( $445\text{ s}^{-1}$ ) and clay (1.5 wt%) in tensile modulus is found to be 98% when compared with a neat epoxy system tested at quasi-static loading.

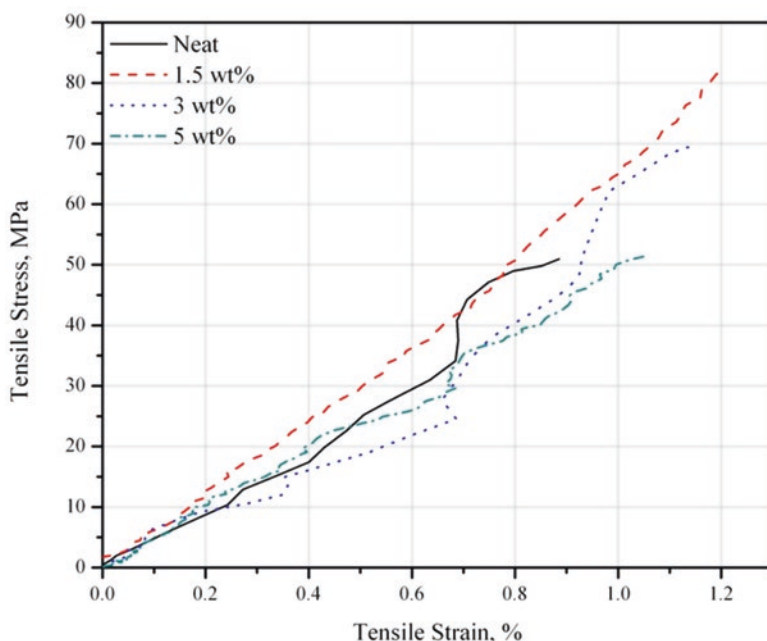


Fig. 3.10 Stress–strain responses of epoxy and its clay nanocomposites at a strain rate of  $385\text{ s}^{-1}$



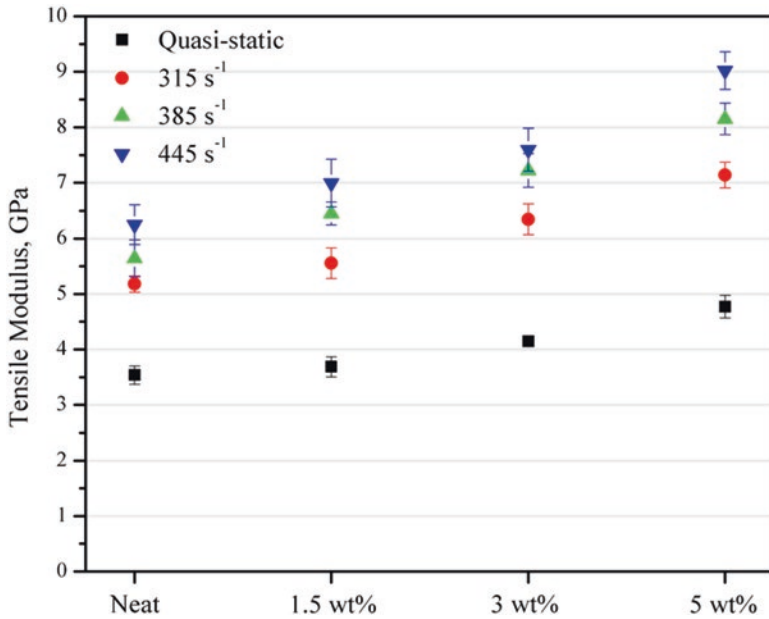


Fig. 3.11 Effect of clay in epoxy on tensile modulus for various high strain rates

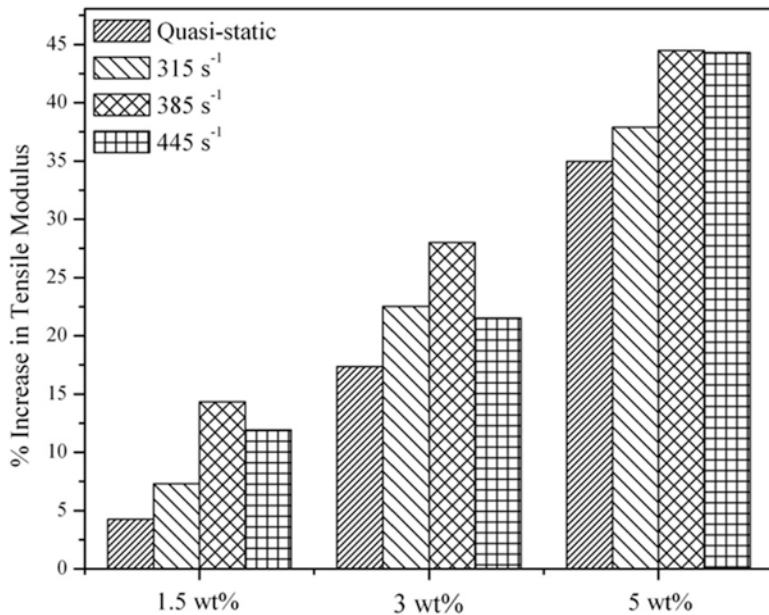
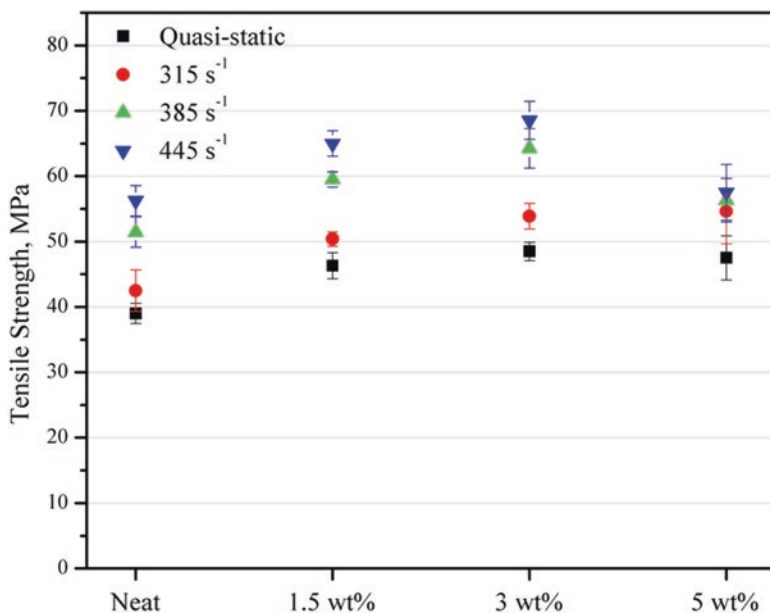


Fig. 3.12 Percentage increase in tensile modulus for various clay loadings in epoxy at quasi-static and dynamic loadings



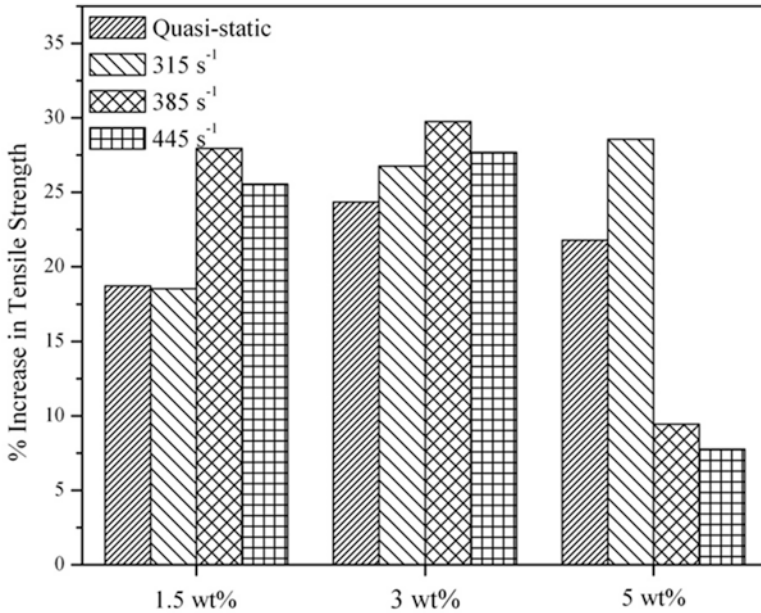
**Fig. 3.13** Effect of clay in epoxy on tensile strength for various high strain rates

Figure 3.13 shows the effect of clay on tensile strength at quasi-static and dynamic loadings and the optimal clay loading is found to be 3.0 wt%. An increment of 25% in tensile strength is observed with the addition of clay at quasi-static loading. At the highest strain rate (445 s<sup>-1</sup>), a 27% increase in tensile strength is observed with the addition of clay in epoxy. The decrease in tensile strength is found at 5.0 wt% clay loading, which could be due to the microvoids and also increased brittleness of the system on addition of clay (Yasmin et al., 2003; Liu et al., 2005; Qi et al., 2006).

Figure 3.14 shows the percentage variation in tensile strength due to the addition of clay in epoxy at quasi-static and dynamic loadings. 3.0 wt% clay/epoxy samples show maximum improvement in strength at all strain rates. The combined effect of high strain rate (445 s<sup>-1</sup>) and clay (1.5 wt%) on the tensile strength is found to be an increase of 67% when compared with a neat epoxy system tested at quasi-static loading.

### 3.3 High Strain Rate Sensitivity of Glass/Epoxy Hybrid Nanocomposites

Dynamic tensile studies were performed in the drop mass tower with a drop mass of 1 kg. Similar to epoxy/clay nanocomposites, three different heights were chosen, viz. 0.5 m, 0.75 m and 1 m, corresponding to high strain rates of 315 s<sup>-1</sup>, 385 s<sup>-1</sup> and

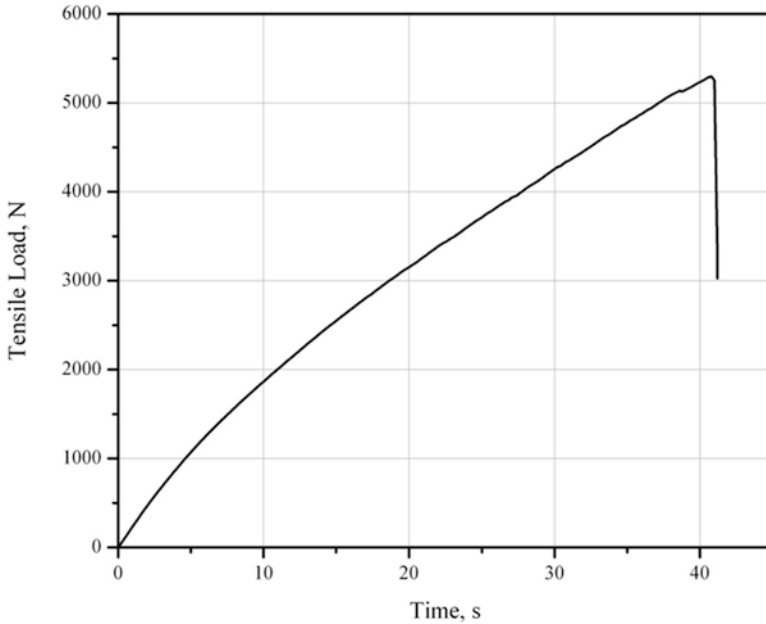


**Fig. 3.14** Percentage increase in tensile strength for various clay loadings in epoxy at quasi-static and dynamic loadings

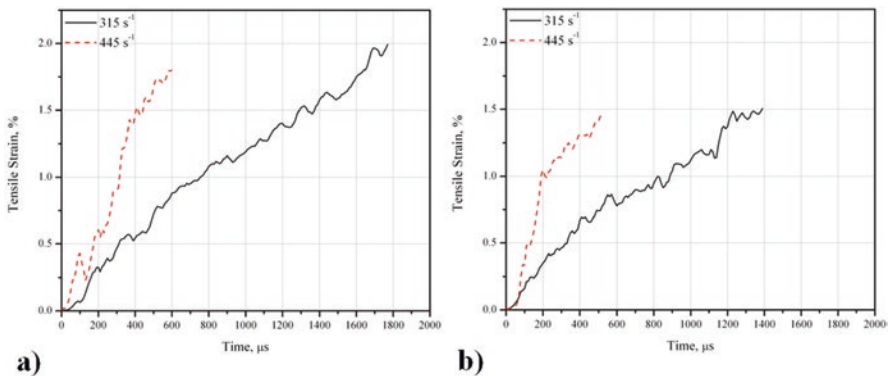
445 s<sup>-1</sup>, respectively, to study the strain rate effects of glass/epoxy composites and its clay nanocomposites (1.5, 3.0 and 5.0 wt%). At quasi-static loading, the stress–strain behaviour is approximately linearly elastic up to the maximum stress point of 315 MPa followed by a sudden failure at a strain of 2.5% (Fig. 3.15).

Figure 3.16 shows the strain histories of 1.5 wt% and 5.0 wt% glass/epoxy/clay nanocomposites tested at drop heights of 0.5 m and 1 m. For 1.5 wt% clay loading, the specimen failed at 2% (1800  $\mu$ s) and 1.8% (600  $\mu$ s) under strain rates of 315 s<sup>-1</sup> and 445 s<sup>-1</sup>, respectively. It is observed that the initial slope of the strain history is not a true indication of the effective strain rate experienced by the material, and hence, the actual strain rates are determined from the gradient of the strain–time curves (Hsiao & Daniel, 1998). The averages of actual strain rates determined at heights of 0.5, 0.75 and 1 m were 24, 41 and 52 s<sup>-1</sup>, respectively. However, the actual strain rates are used in practice for analysis. In general, the nominal or theoretical strain rate can be calculated by dividing the gauge length of the specimen to the cross-head speed (here, it is drop mass velocity).

Figure 3.17 shows the strain contour plots of 1.5 wt% clay/glass/epoxy nanocomposites at a strain rate of 315 s<sup>-1</sup>. A strain localization is observed just before the failure, which indicates the physical phenomena and not due to DIC parameters. The longitudinal strain ( $\epsilon_{yy}$ ) distribution at  $t_0 + 460 \mu$ s corresponding to a load value of 283 N is shown in Fig. 3.17a. Similarly, Fig. 3.17b shows strain distribution at  $t_0 + 1460 \mu$ s corresponding to a load value of 1080 N.



**Fig. 3.15** A typical load history of glass/epoxy composite at quasi-static loading



**Fig. 3.16** Strain histories of (a) 1.5 wt% and (b) 5.0 wt% clay/glass/epoxy nanocomposites for various high strain rates (Gurusideswar et al., 2017), copyright 2021. Reproduced with permission from Elsevier Ltd.

Figure 3.18 shows the stress–strain response for neat glass/epoxy and 5.0 wt% glass/epoxy/clay nanocomposites at quasi-static and dynamic loading. The stress–strain behaviour shows increasing slope and strength and decreasing strain with the increase of strain rate. The strain rate effects of polymers can be explained by the shape of the stress–strain curves (Gilat et al., 2007).

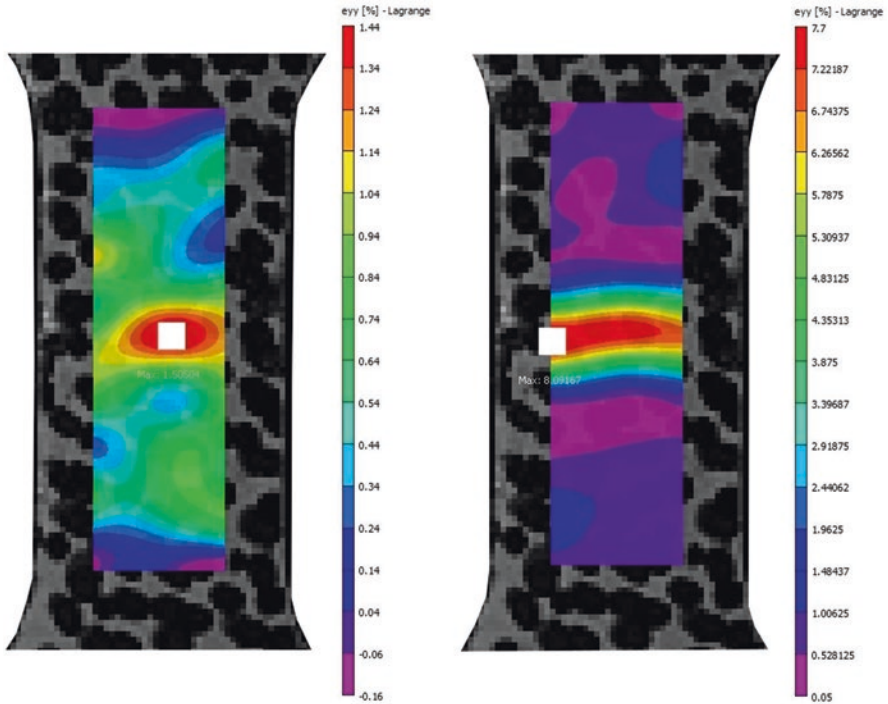


**Fig. 3.17** Strain contour plots of 1.5 wt% clay/glass/epoxy nanocomposites at a strain rate of  $315 \text{ s}^{-1}$  (Gurusideswar et al., 2017), copyright 2021. Reproduced with permission from Elsevier Ltd.

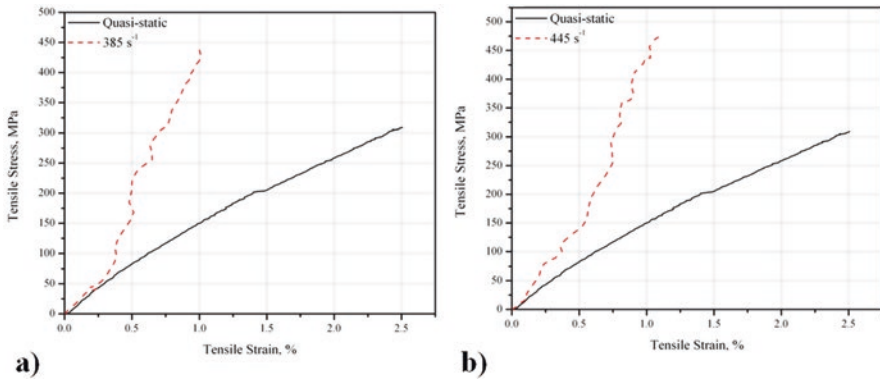


**Fig. 3.18** Stress–strain response of (a) neat and (b) 5.0 wt% glass/epoxy composite at quasi-static and dynamic loadings

### 3.3.1 Effect of High Strain Rate on Tensile Properties of Glass/Epoxy

The tensile modulus, strength and strain to failure at various high strain rates are presented in Table 3.2 for neat glass/epoxy, 1.5, 3.0 and 5.0 wt% glass/epoxy/clay nanocomposites, respectively. It is observed that the tensile modulus is relatively sensitive to high strain rates.

The variation of tensile modulus and strength with the log of strain rate (Fig. 3.19) shows a sharp upward deviation in the high strain rate region, which confirms the strain rate sensitivity of the material. The values of tensile modulus and tensile strength of glass/epoxy composites obtained at low strain rates ( $10^{-4}$ – $10^{-1}$  s $^{-1}$ ) are also included in Fig. 3.19 for comparison.

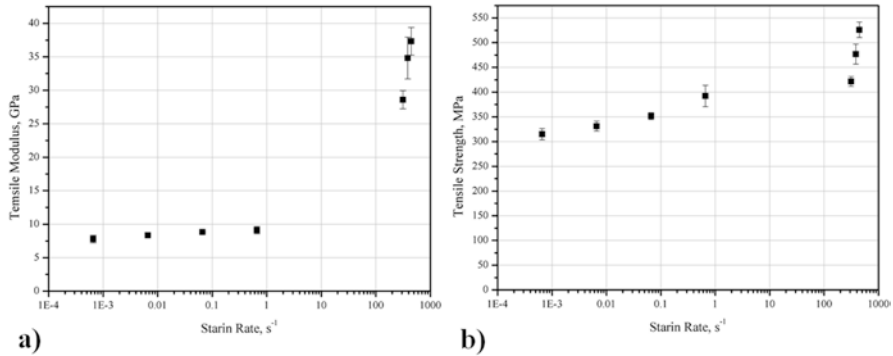
Figure 3.20 shows load histories of 1.5 wt% and 3.0 wt% glass/epoxy/clay nanocomposites at high strain rates (315–445 s $^{-1}$ ). 3.0 wt% clay samples show a higher load of 1550 N, whereas 1.5 wt% clay samples show 1400 N at the highest strain rate of 445 s $^{-1}$ .

Figure 3.21 illustrates the effect of strain rate on the tensile modulus of glass/epoxy/clay nanocomposites. The tensile modulus (18.09 GPa) increases significantly by 106% (37.31 GPa) for the highest strain rate of neat glass/epoxy composites. The same trend is followed for glass/epoxy/clay nanocomposites. An increase of 150%, 173% and 158% in tensile modulus is observed from quasi-static to the highest strain rate of 445 s $^{-1}$  for 1.5, 3.0 and 5.0 wt% clay loadings, respectively.

Figure 3.22 illustrates the effect of strain rate on the tensile strength of glass/epoxy/clay nanocomposites. The tensile strength is relatively sensitive to high strain rates. The tensile strength (314.9 MPa) increases up to 67% (526 MPa) for the strain

**Table 3.2** Effect of high strain rate on tensile properties of glass/epoxy/clay nanocomposites

Clay content wt%	Drop mass height m	Strain rate s $^{-1}$	Tensile modulus GPa	Tensile strength MPa	Tensile strain %
Neat	Quasi-static	0.001	18.09 ± 0.17	314.9 ± 0.71	2.507 ± 0.02
	0.5	315	28.58 ± 1.36	421.7 ± 10.1	2.272 ± 0.212
	0.75	385	34.81 ± 3.13	476.9 ± 20.2	1.942 ± 0.225
	1	445	37.31 ± 2.06	526.1 ± 15.8	1.798 ± 0.023
1.5	Quasi-static	0.001	19.65 ± 0.18	343.2 ± 3.1	1.693 ± 0.04
	0.5	315	32.61 ± 2.99	446.5 ± 8.1	1.746 ± 0.206
	0.75	385	40.75 ± 4.3	529.9 ± 21.6	1.635 ± 0.128
	1	445	45.2 ± 2.13	579.5 ± 14.4	1.476 ± 0.019
3	Quasi-static	0.001	20.13 ± 0.07	326.8 ± 2.8	1.771 ± 0.08
	0.5	315	33.05 ± 1.26	443.2 ± 6.3	1.663 ± 0.18
	0.75	385	43.07 ± 5.05	510.3 ± 21.5	1.54 ± 0.188
	1	445	49.36 ± 6.33	573.9 ± 29.8	1.131 ± 0.058
5	Quasi-static	0.001	19.35 ± 0.21	321.7 ± 3.7	1.894 ± 0.09
	0.5	315	29.65 ± 0.92	432.6 ± 4.7	1.599 ± 0.083
	0.75	385	40.36 ± 1.76	479.6 ± 17.2	1.513 ± 0.12
	1	445	46.69 ± 3.38	530.7 ± 18.5	1.087 ± 0.094



**Fig. 3.19** Variation in (a) tensile modulus and (b) tensile strength with log of strain rate for glass/epoxy composites (Gurusideswar et al., 2017), copyright 2021. Reproduced with permission from Elsevier Ltd.

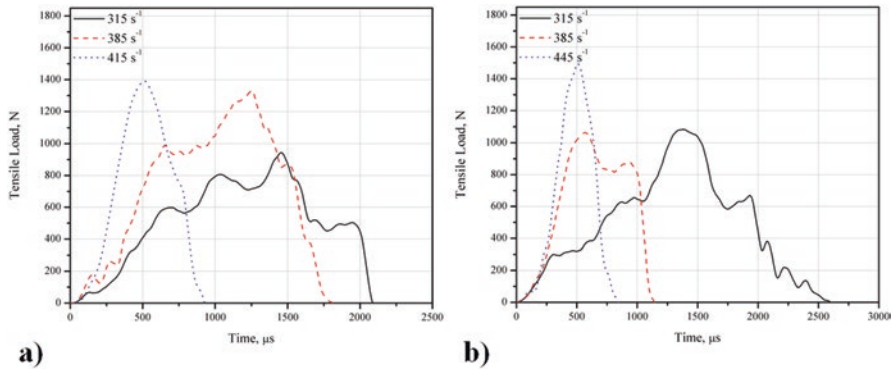


**Fig. 3.20** Load histories of (a) 1.5 wt% and (b) 3.0 wt% clay/glass/epoxy nanocomposites for various high strain rates (Gurusideswar et al., 2017), copyright 2021. Reproduced with permission from Elsevier Ltd.

rate of  $445 \text{ s}^{-1}$  of neat glass/epoxy composites. A similar trend of increase in tensile strength with strain rate is in agreement with the findings of Okoli and Smith (2000). The increase in tensile strength and modulus is ascribed to the viscoelastic nature of the matrix, fibre–matrix interfacial properties, weaving type and geometry of the composites (Welsh & Harding, 1985; Brown et al., 2010). An increase of 69%, 76% and 65% in tensile strength is observed from quasi-static to the strain rate of  $445 \text{ s}^{-1}$  for 1.5, 3.0 and 5.0 wt% clay loadings, respectively.

From the results, it is observed that the stiffness of glass/epoxy/clay nanocomposites is more sensitive to strain rates compared to its tensile strength. On average, a 25% decrease in failure strain is found as strain rate increases for glass/epoxy/clay nanocomposites. Similar observations were observed by many researchers. Majzoobi et al. (2005) observed nearly 50% decrease of failure strain for  $[\pm 60^\circ]$  glass/epoxy composites at  $621 \text{ s}^{-1}$ , and Ochola et al. (2004) observed a strain to

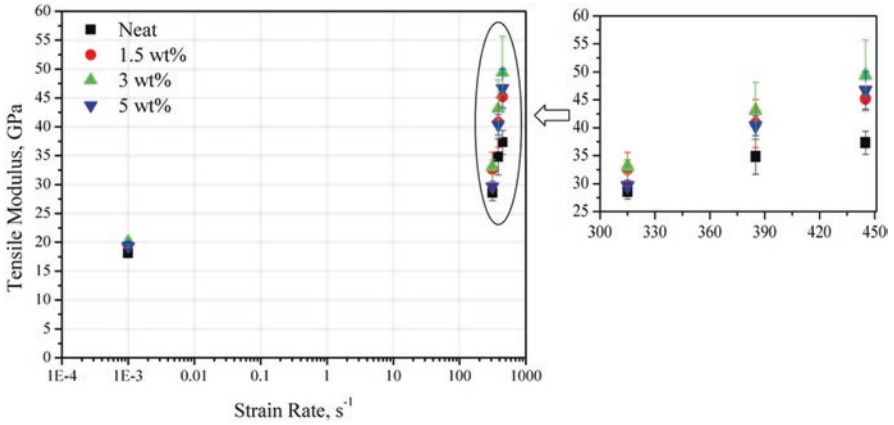


Fig. 3.21 Effect of high strain rate on tensile modulus of glass/epoxy/clay nanocomposites

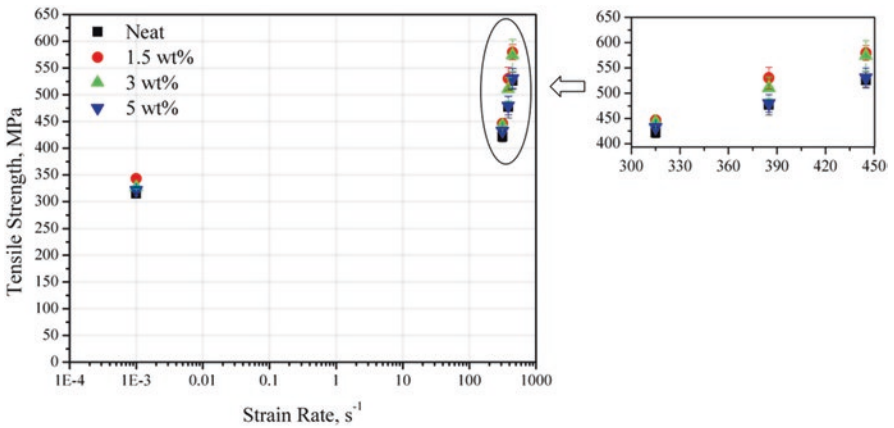


Fig. 3.22 Effect of high strain rate on tensile strength of glass/epoxy/clay nanocomposites

failure of 15% under compression loading at low strain rates ( $10^{-3} \text{ s}^{-1}$ ) and 4% at high strain rate of  $450 \text{ s}^{-1}$  for GFRP system. It is believed that due to rapid loading, the composite tends to be more brittle resulting in a lower strain to failure.

### 3.3.2 Effect of Clay on Tensile Properties of Glass/Epoxy

The addition of nanoclay makes the glass/epoxy nanocomposites fail in a brittle mode (Fig. 3.23) and leads to restriction of plastic deformations in the nanocomposites (Kornmann et al., 2005). From Fig. 3.24, an increment of 15% in tensile modulus is achieved with the addition of 3.0 wt% of clay in glass/epoxy at quasi-static loading. At high strain rate ( $445 \text{ s}^{-1}$ ), 25% increase in tensile modulus is observed



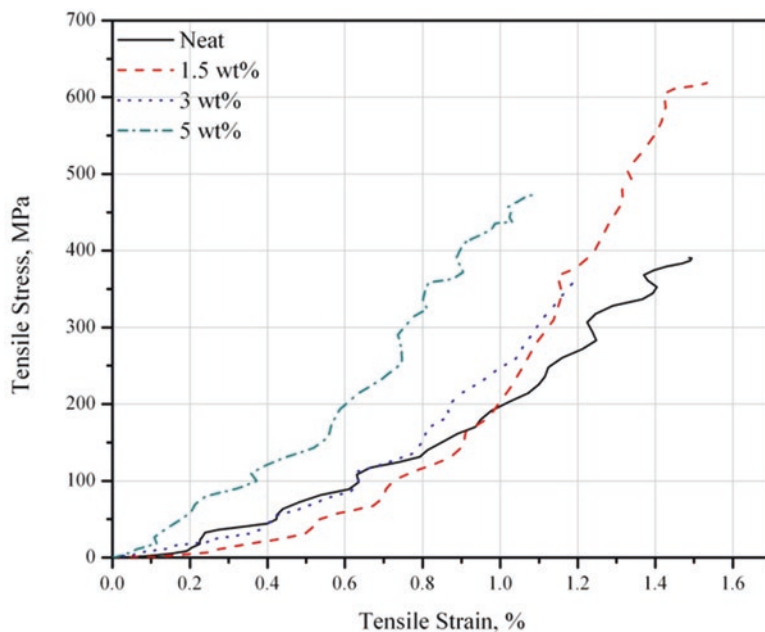


**Fig. 3.23** Stress–strain responses of glass/epoxy and its clay nanocomposites at a strain rate of  $445 \text{ s}^{-1}$  (Gurusideswar et al., 2017), copyright 2021. Reproduced with permission from Elsevier Ltd.

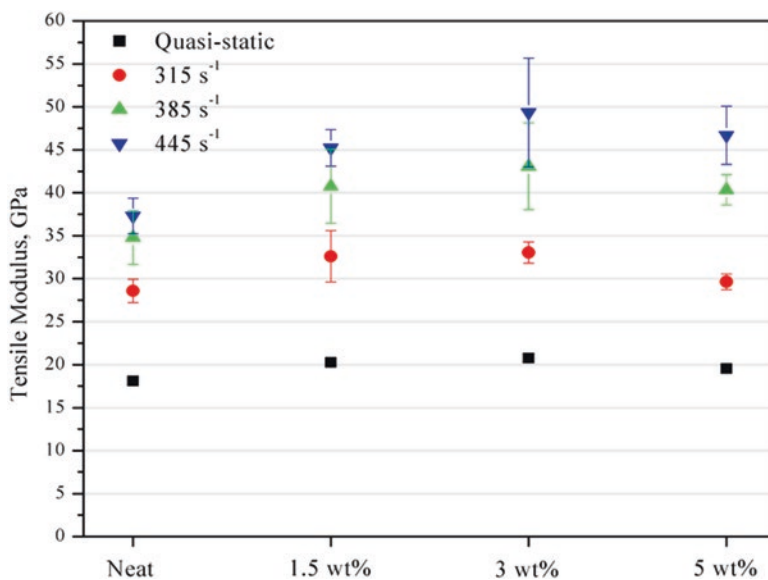


**Fig. 3.24** Effect of clay on tensile modulus at different high strain rates

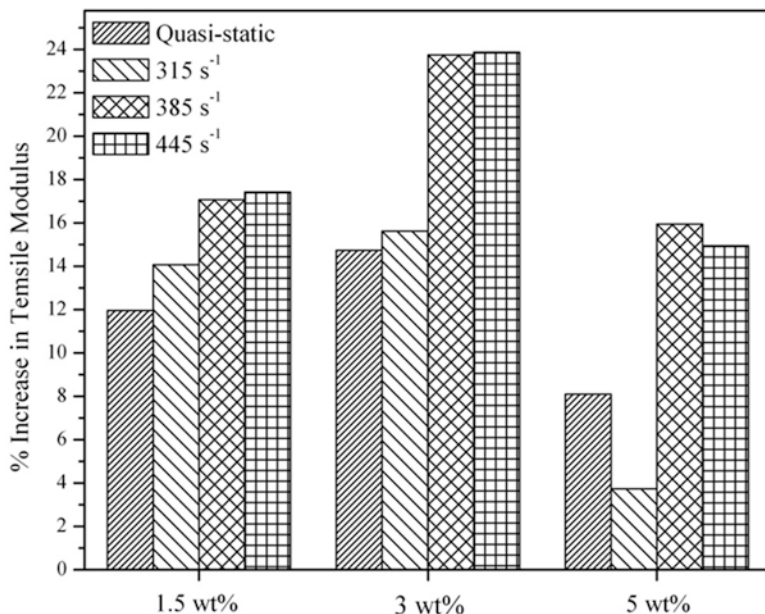


**Fig. 3.25** Percentage increase in tensile modulus for various clay loadings in glass/epoxy at quasi-static and dynamic loadings (Gurusideswar et al., 2017), copyright 2021. Reproduced with permission from Elsevier Ltd.

with the addition of 3.0 wt% of clay in glass/epoxy composites. Similarly, a maximum increment of 24% and 16% in tensile modulus is found at strain rates of 385 s<sup>-1</sup> and 315 s<sup>-1</sup> by adding 3.0 wt% of clay in glass/epoxy composites. Similar findings are reported by many authors (Wu et al., 2002; Yasmin et al., 2006; Shi et al., 2009; Zainuddin et al., 2010). It is also noted that the microstructure of glass fibre/epoxy/clay restricts the mobility of the polymer in the interface between the fibre and epoxy or between the clay and epoxy in the glass/epoxy/clay nanocomposites. This allows better stress transfer to the fibres and leads to an improved stiffness at low strain values (Lin et al., 2006).

Figure 3.25 shows the percentage variation in tensile modulus due to the addition of clay in glass/epoxy at quasi-static and dynamic loadings. 3.0 wt% glass/epoxy/clay sample shows maximum improvement at all strain rates. The combined effect of high strain rate (445 s<sup>-1</sup>) and clay (1.5 wt%) in tensile modulus is found to be 150% when compared with neat glass/epoxy composites tested at quasi-static loading.

Similarly, the tensile strength increases with increasing clay loading. Figure 3.26 shows the effect of clay on tensile strength at quasi-static and dynamic loadings. An increment of 9% in tensile strength is observed with the addition of 1.5 wt% clay at quasi-static loading. However, at higher clay loadings, the tensile strength decreases. The reason for the decrement could be the formation of clay agglomerations, which leads to stress concentration, thus causing premature failure and formation of

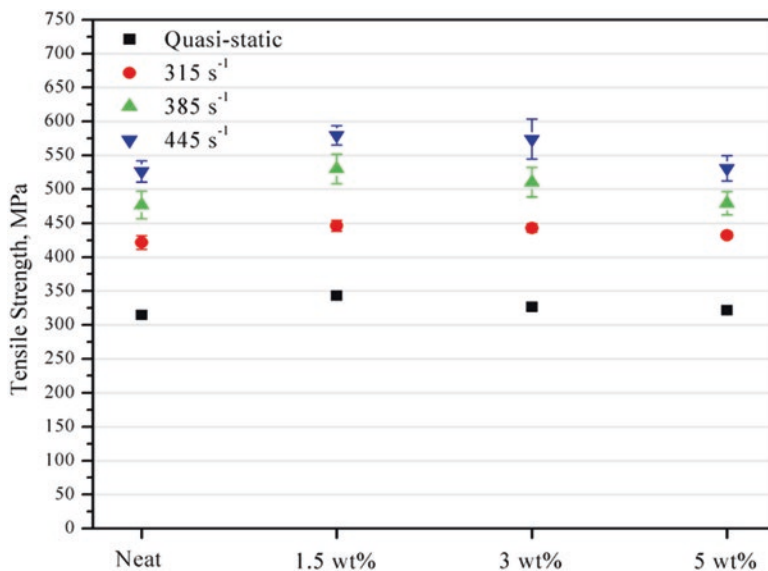


Fig. 3.26 Effect of clay on tensile strength for various strain rates

microvoids at higher clay loadings. At the highest strain rate ( $445 \text{ s}^{-1}$ ), 10% increase in tensile strength is observed with the addition of 1.5 wt% of clay in glass/epoxy composites. Similarly, a maximum increase of 11% and 6% in tensile strength is observed at strain rates of  $385 \text{ s}^{-1}$  and  $315 \text{ s}^{-1}$  by adding 1.5 wt% of clay in glass/epoxy composites.

Figure 3.27 shows the percentage variation in tensile strength due to the addition of clay in glass/epoxy at quasi-static and dynamic loadings. Optimal clay loading of 1.5 wt% is identified at quasi-static and dynamic tensile loadings. The combined effect of high strain rate ( $445 \text{ s}^{-1}$ ) and clay (1.5 wt%) in tensile strength is found to be 84% when compared with neat glass/epoxy composites tested at quasi-static loading.

### 3.4 Fractography

Fractography of the failed specimens was investigated using HR-SEM (Hitachi model S-4800) to study the effects of clay addition and high strain rate on tensile properties of epoxy and glass/epoxy composites. The SEM micrograph (Fig. 3.28) shows a smooth, glassy and featureless fracture surface for a neat epoxy specimens tested at quasi-static loading. This type of morphology indicates a typical brittle fracture behaviour of epoxy resin (Ratna et al., 2003; Zhou et al., 2006; Wang et al., 2006; Zainuddin et al., 2010).

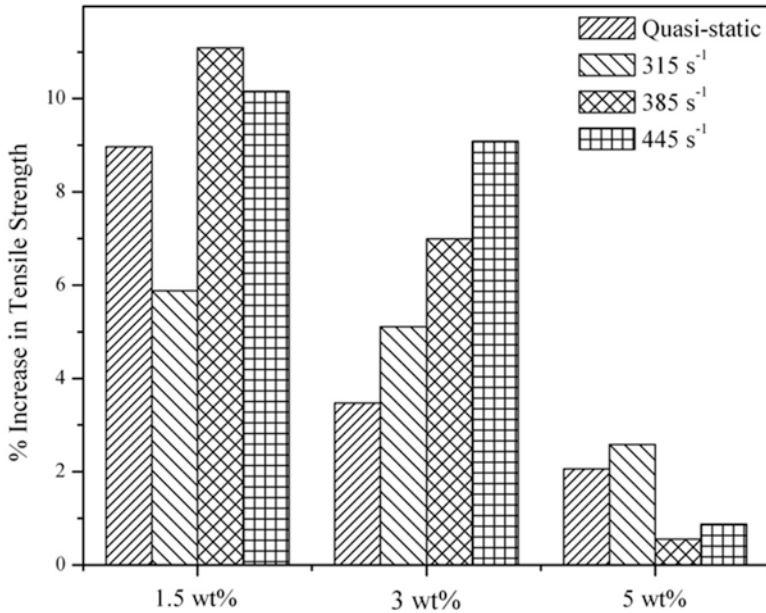


**Fig. 3.27** Percentage increase in tensile strength for various clay loadings at quasi-static and dynamic loadings (Gurusideswar et al., 2017), copyright 2021. Reproduced with permission from Elsevier Ltd.

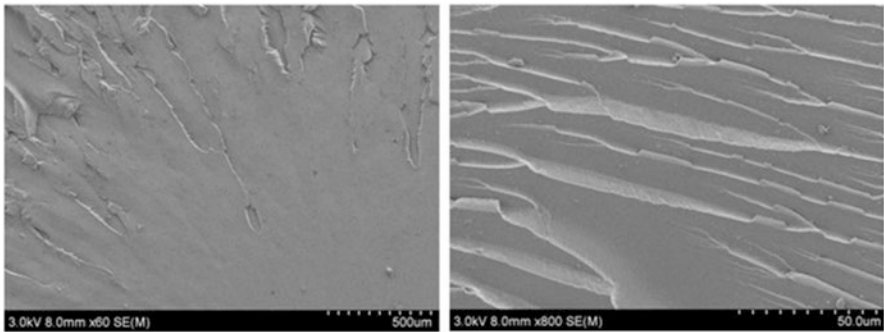


**Fig. 3.28** SEM images of tensile fractured surfaces of neat epoxy at different magnifications in quasi-static loading (Gurusideswar et al., 2016), copyright 2021. Reproduced with permission from Elsevier Ltd.

The fracture surfaces of epoxy/clay nanocomposites (Fig. 3.29) show rough fractographic features, deep river markings and clay agglomerates. The increased surface roughness shows that the crack path is more distorted and difficult to propagate due to the presence of nanoclay (Wang et al., 2006). Also, cleavages are observed on fracture surfaces of epoxy and its clay nanocomposites. Deep cleavages are observed in neat epoxy specimens, whereas shallow cleavages are observed in

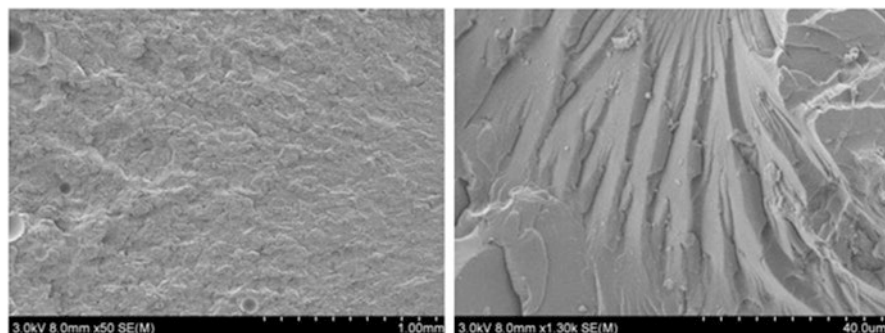


**Fig. 3.29** Fractured surfaces of 1.5 wt% clay/epoxy nanocomposites at different magnifications in quasi-static loading (Gurusideswar et al., 2016), copyright 2021. Reproduced with permission from Elsevier Ltd.

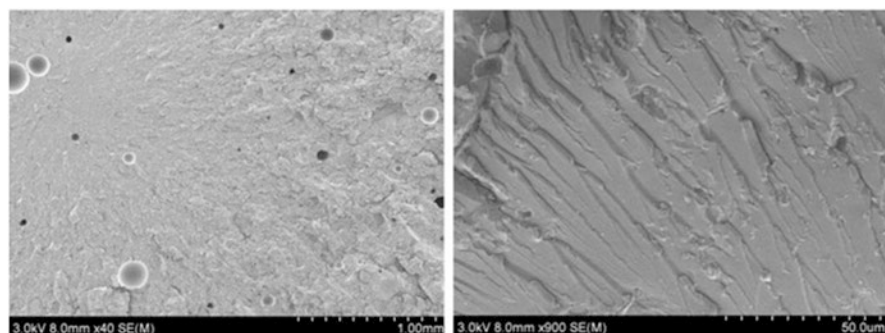


**Fig. 3.30** Fractured surfaces of 3.0 wt% clay/epoxy nanocomposites at different magnifications in quasi-static loading (Gurusideswar et al., 2016), copyright 2021. Reproduced with permission from Elsevier Ltd.

epoxy/clay nanocomposite specimens. In addition, microvoids are observed in epoxy/clay nanocomposites containing higher clay content (Fig. 3.30), and also the failure mode is significantly changed as shown in Figs. 3.29 and 3.30. The failure is initiated at a localized domain which might be due to the presence of agglomerations of clay particles, and the crack initiation is caused by the stress concentration developed around the agglomerated particles leading to failure (Zainuddin et al., 2010).

It is observed that the roughness of the fracture surface has increased considerably at higher strain rates due to irregular deep cleavages, resulting in sudden failure (Shadlou et al., 2014). Similar to quasi-static testing, epoxy/clay nanocomposites exhibit rough fractographic features in dynamic tensile testing. Figure 3.31 shows the micrograph of neat epoxy at  $385 \text{ s}^{-1}$ , which resembles a typical cleavage fracture. With the addition of clay, the fracture surface shows secondary cracks and more and deeper river markings around the agglomerates.

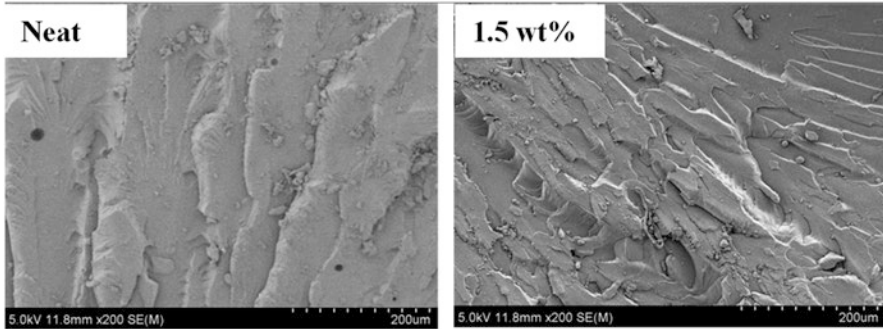


**Fig. 3.31** Fractured surfaces of neat epoxy and its clay nanocomposites at a strain rate of  $385 \text{ s}^{-1}$  at low magnification (Gurusideswar et al., 2016), copyright 2021. Reproduced with permission from Elsevier Ltd.

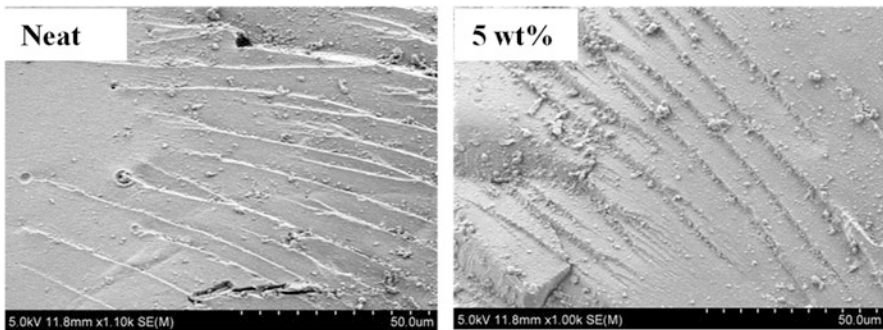


**Fig. 3.32** Fractured surfaces of neat epoxy and its clay nanocomposites at a strain rate of  $385 \text{ s}^{-1}$  at high magnification (Gurusideswar et al., 2016), copyright 2021. Reproduced with permission from Elsevier Ltd.

The fracture surface of epoxy/clay nanocomposites at high magnification (Fig. 3.32) shows massive shear deformation. This indicates that during loading the stress concentration developed around the nanoparticles contributed to shear yielding of epoxy interlayers at the tip of the propagating crack (Ratna et al., 2003). Cavities are observed in 3.0 wt% clay content (Fig. 3.33), and this might be due to entrapped voids or decohesion of clay agglomerations after failure (Yasmin et al., 2003; Liu et al., 2005; Qi et al., 2006). Also, the fracture surface of nanocomposites with 5.0 wt% of clay content confirms that the formation of microvoids was due to the debonding of clay nanoparticles from the matrix.

Similar to epoxy/clay nanocomposites, fractography of the failed specimens was investigated using HR-SEM (Hitachi model S-4800) to study the effects of clay addition and high strain rate on tensile properties of glass/epoxy composites. Figure 3.34 shows fibre–matrix interactions of different clay loadings at quasi-static loading. From Fig. 3.34, it is observed that the fibres are de-bonded from the matrix and fibre breaking is the dominant mode of failure for neat glass/epoxy, which

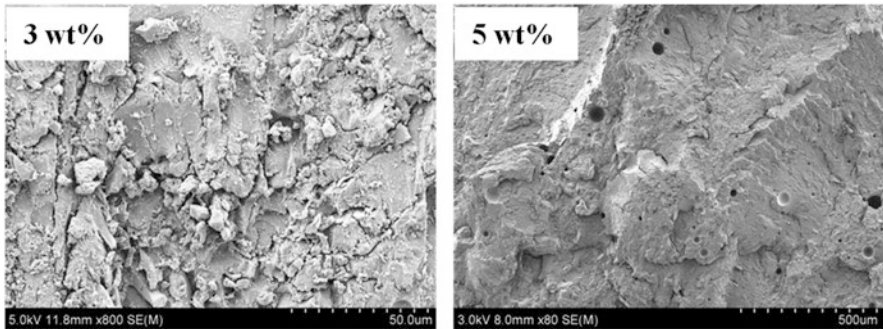


**Fig. 3.33** SEM micrographs of 3.0 wt% and 5.0 wt% clay/epoxy nanocomposites reveal microvoids at different magnifications (Gurusideswar et al., 2016), copyright 2021. Reproduced with permission from Elsevier Ltd.

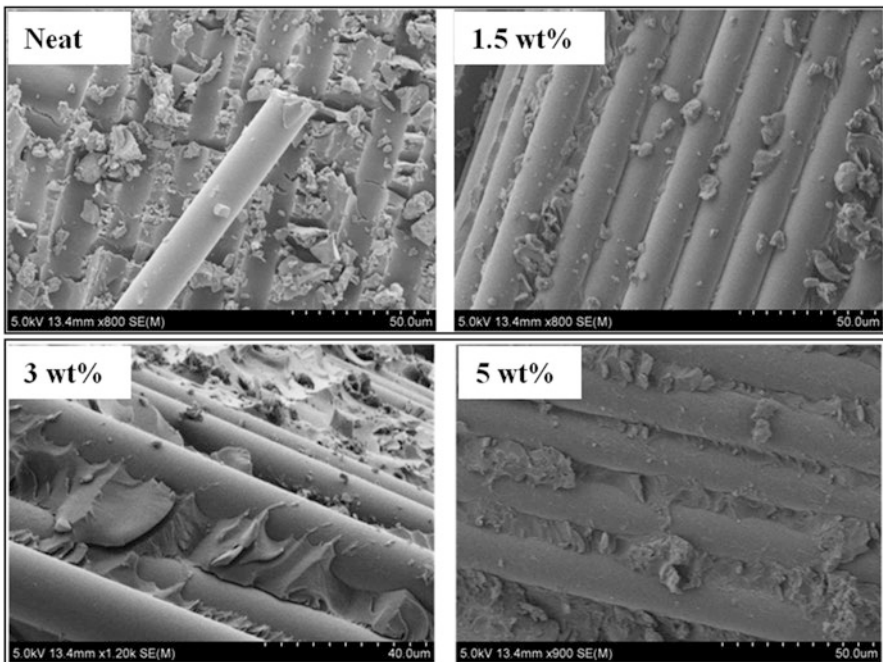


**Fig. 3.34** Fibre matrix interaction of glass/epoxy and its clay nanocomposites (Gurusideswar et al., 2017), copyright 2021. Reproduced with permission from Elsevier Ltd.

indicates poor adhesion between fibre and matrix. In the case of glass/epoxy composites with clay, it is clearly observed that the surface of the fibres is rougher and the fibres have good bonding with the matrix (Chowdhury et al., 2006; Shi et al., 2009; Khan et al., 2011). Figure 3.34 shows good wettability between matrix and fibre of 1.5 wt% and 3.0 wt% clay loadings. This could be due to the particular

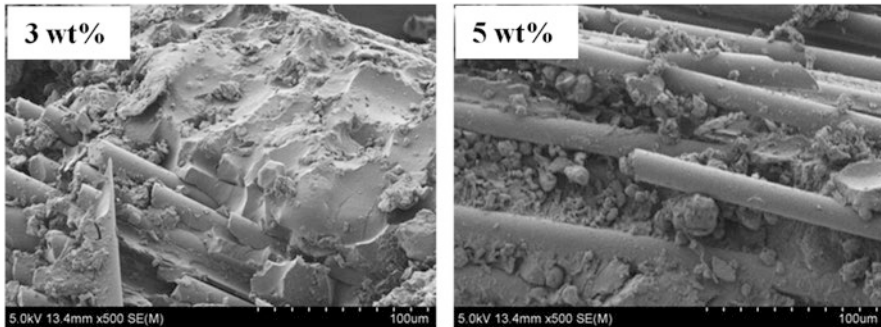


**Fig. 3.35** Fracture surfaces of glass/epoxy/clay nanocomposites show matrix agglomeration (Gurusideswar et al., 2017), copyright 2021. Reproduced with permission from Elsevier Ltd.

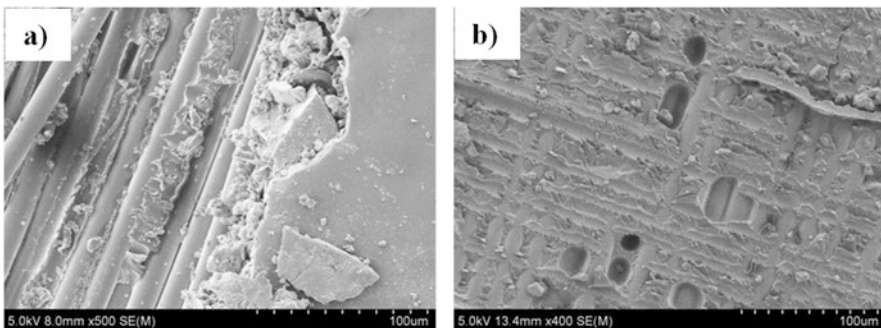


**Fig. 3.36** SEM micrographs of (a) matrix damage and (b) minor agglomerations (Gurusideswar et al., 2017), copyright 2021. Reproduced with permission from Elsevier Ltd.

affinity of the nanoclay with the glass fibre surface. It is explained by Kornmann et al. (2005) that both fibres and clay are inorganic materials functionalized at the surface with organic molecules, which lead to polarity match between their respective surfaces.

At higher clay loadings (Fig. 3.35), coarse surface and matrix agglomeration are observed in the fibre–matrix interface region resulting in improved interfacial bonding strength (Haque et al., 2003). The increase in clay loading prevents the free volume of nanoparticles from moving around and the cross-link density of the epoxy is increased leading to a tendency to form clay clusters or agglomerates (Lam et al., 2005). Quaresimin and Varley (2008) found a similar morphology for 3.0 wt% nanomodified epoxy laminate and stated an improved local energy dissipation for the nanomodified laminates.

Figure 3.36 shows matrix damage and agglomeration of neat and 1.5 wt% clay glass/epoxy nanocomposites, respectively. The rough fracture surface induced by the addition of clay indicates the enhanced interfacial bonding of the clay with matrix and the clay with fibre, which results in improvement in tensile modulus. The



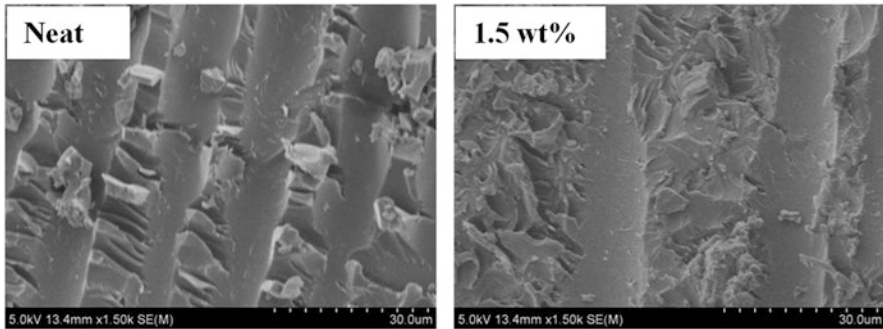


**Fig. 3.37** SEM micrographs show fibre pull-outs at a strain rate of  $445 \text{ s}^{-1}$  (Gurusideswar et al., 2017), copyright 2021. Reproduced with permission from Elsevier Ltd.

microvoids and the clay agglomeration at higher clay loadings lead to a decrease in tensile strength.

It is noted that the fibre pull-outs are dominant with increasing strain rates (Fig. 3.37). Also, the interfacial debonding becomes more severe with increasing strain rate. Staab and Gilat (1995) observed significant changes in the fracture surface appearance as a function of strain rate, and Shokrieh and Omidi (2009) also reported significant changes in the fracture surface with the increase in strain rate by visually inspecting the failed specimens of glass/epoxy composites.

## 4 Conclusions

The prime objective of this research work was to study the strain rate effects of epoxy, glass/epoxy and its clay nanocomposites. Composite materials are widely used in aerospace structures, automotive industry and marine structures, and in many instances, they are subjected to high-velocity dynamic loadings, which require prior knowledge of dynamic mechanical properties to prevent catastrophic failure at high loading rates. Numerous literatures on high strain rate effects for epoxy and glass/epoxy composites using split-Hopkinson pressure bar (SHPB) have been reported earlier. But the strain rate effects of composites in the medium range ( $100\text{--}1000 \text{ s}^{-1}$ ) are rarely reported. Hence, the high strain rate effects of epoxy, glass/epoxy and its clay nanocomposites are considered for the current research work and investigated.

Dynamic tensile studies were conducted on epoxy/clay and glass/epoxy/clay nanocomposites, using a drop mass setup equipped with in-house fabricated specimen fixture assembly and a high-speed camera. Data obtained from this method filled a gap between conventional testing machines and SHPB measurements. The effects of the strain rate and clay on the tensile behaviour of epoxy resin and glass/epoxy composite were investigated over a wide range of strain rates. A non-contact

strain measurement technique (DIC) using the high-speed camera was employed to capture the full-field strain measurement in the dynamic environment. Quasi-static and dynamic experiment results show that the tensile behaviour of epoxy/clay nanocomposites is dependent on the strain rate. When the strain rate increases from 0.008 to 445 s<sup>-1</sup>, the tensile modulus (+67%) and tensile strength (+45%) increased for the neat epoxy system and the modulus (106%) and strength (+67%) for neat glass/epoxy composite. A similar trend is observed for epoxy, glass/epoxy and its clay nanocomposites. The presence of clay in epoxy and glass/epoxy composite plays a significant role during dynamic loading. Microscopic observations of the fracture surface showed that the surface becomes rougher with the increase in strain rate. The fracture surfaces of epoxy and glass/epoxy composites were studied using SEM to understand the strain rate effects. The roughness of the fracture surface for epoxy is increased at higher strain rates, leading to irregular cleavages and deeper valleys; these signify sudden fractures. In the case of glass/epoxy, with increasing strain rate, fracture path covers the entire gauge region and an extensive debonding of fibres from the matrix is observed.

Material behaviour at high strain rates obtained through experimental methods can be used for validation of proposed material models, and the future scope of this work is focused on the development of test standards for the determination of dynamic mechanical properties.

## References

- Alsubari, S., Zuhri, M. Y. M., Sapuan, S. M., et al. (2021). Potential of natural fiber reinforced polymer composites in sandwich structures: A review on its mechanical properties. *Polymers*, 13, 423. <https://doi.org/10.3390/polym13030423>
- Armenàkas, A. E., & Sciammarella, C. A. (1973). Response of glass-fiber-reinforced epoxy specimens to high rates of tensile loading. *Experimental Mechanics*, 13, 433–440. <https://doi.org/10.1007/bf02324887>
- Azeez, A. A., Rhee, K. Y., Park, S. J., & Hui, D. (2013). Epoxy clay nanocomposites—Processing, properties and applications: A review. *Composites Part B: Engineering*, 45, 308–320. <https://doi.org/10.1016/j.compositesb.2012.04.012>
- Barré, S., Chotard, T., & Benzeggagh, M. L. (1996). Comparative study of strain rate effects on mechanical properties of glass fibre-reinforced thermoset matrix composites. *Composites Part A: Applied Science and Manufacturing*, 27, 1169–1181.
- Brown, K. A., Brooks, R., & Warrior, N. A. (2010). The static and high strain rate behaviour of a commingled E-glass/polypropylene woven fabric composite. *Composites Science and Technology*, 70, 272–283. <https://doi.org/10.1016/j.compscitech.2009.10.018>
- Buckley, C. P., Harding, J., Hou, J. P., et al. (2001). Deformation of thermosetting resins at impact rates of strain. Part I: Experimental study. *Journal of the Mechanics and Physics of Solids*, 49, 1517–1538. [https://doi.org/10.1016/S0022-5096\(00\)00085-5](https://doi.org/10.1016/S0022-5096(00)00085-5)
- Cao, K., Ma, X., Zhang, B., et al. (2010). Tensile behavior of polycarbonate over a wide range of strain rates. *Materials Science and Engineering A*, 527, 4056–4061. <https://doi.org/10.1016/j.msea.2010.03.088>
- Chen, W., Lu, F., & Cheng, M. (2002). Tension and compression tests of two polymers under quasi-static and dynamic loading. *Polymer Testing*, 21, 113–121. [https://doi.org/10.1016/S0142-9418\(01\)00055-1](https://doi.org/10.1016/S0142-9418(01)00055-1)

- Chowdhury, F. H. H., Hosur, M. V. V., & Jeelani, S. (2006). Studies on the flexural and thermomechanical properties of woven carbon/nanoclay-epoxy laminates. *Materials Science and Engineering A*, 421, 298–306. <https://doi.org/10.1016/j.msea.2006.01.074>
- Clifton, S., Thimmappa, B. H. S., Selvam, R., & Shivamurthy, B. (2020). Polymer nanocomposites for high-velocity impact applications-A review. *Composites Communications*, 17, 72–86. <https://doi.org/10.1016/j.coco.2019.11.013>
- Daniel, I. M., LaBedz, R. H., & Liber, T. (1981). New method for testing composites at very high strain rates. *Experimental Mechanics*, 21, 71–77. <https://doi.org/10.1007/bf02325199>
- Davies, R. G., & Magee, C. L. (1975). The effect of strain-rate upon the tensile deformation of materials. *Journal of Engineering Materials and Technology, Transactions of the ASME*, 97, 151–155. <https://doi.org/10.1115/1.3443275>
- Elmahdy, A., & Verleysen, P. (2019). Tensile behavior of woven basalt fiber reinforced composites at high strain rates. *Polymer Testing*, 76, 207–221. <https://doi.org/10.1016/j.polymertesting.2019.03.016>
- Evora, V. M. F., & Shukla, A. (2003). Fabrication, characterization, and dynamic behavior of polyester/TiO<sub>2</sub> nanocomposites. *Materials Science and Engineering A*, 361, 358–366. [https://doi.org/10.1016/S0921-5093\(03\)00536-7](https://doi.org/10.1016/S0921-5093(03)00536-7)
- Fu, S., Wang, Y., & Wang, Y. (2009). Tension testing of polycarbonate at high strain rates. *Polymer Testing*, 28, 724–729. <https://doi.org/10.1016/j.polymertesting.2009.06.002>
- Gilat, A., Goldberg, R. K., & Roberts, G. D. (2007). Strain rate sensitivity of epoxy resin in tensile and shear loading. *Journal of Aerospace Engineering*, 20, 75–80. [https://doi.org/10.1061/\(asce\)0893-1321\(2007\)20:2\(75\)](https://doi.org/10.1061/(asce)0893-1321(2007)20:2(75))
- Groves, S., Sanchez, R., Lyon, R., & Brown, A. (1993). High strain rate effects for composite materials. In *Eleventh Volume: Composite materials—Testing and design*. ASTM International.
- Guo, Y., & Li, Y. (2007). Quasi-static/dynamic response of SiO<sub>2</sub>-epoxy nanocomposites. *Materials Science and Engineering A*, 458, 330–335. <https://doi.org/10.1016/j.msea.2007.02.011>
- Gurusideswar, S., Velmurugan, R., & Gupta, N. K. (2016). High strain rate sensitivity of epoxy/clay nanocomposites using non-contact strain measurement. *Polymer*, 86, 197–207. <https://doi.org/10.1016/j.polymer.2015.12.054>
- Gurusideswar, S., Velmurugan, R., & Gupta, N. K. (2017). Study of rate dependent behavior of glass/epoxy composites with nanofillers using non-contact strain measurement. *International Journal of Impact Engineering*, 110, 324–337. <https://doi.org/10.1016/j.ijimpeng.2017.05.013>
- Hamouda, A. M. S., & Hashmi, M. S. J. (1998). Testing of composite materials at high rates of strain: Advances and challenges. *Journal of Materials Processing Technology*, 300, 327–336. [https://doi.org/10.1016/s0924-0136\(97\)00436-6](https://doi.org/10.1016/s0924-0136(97)00436-6)
- Haque, A., Shamsuzzoha, M., Hussain, F., & Dean, D. (2003). S2-glass/epoxy polymer nanocomposites: Manufacturing, structures, thermal and mechanical properties. *Journal of Composite Materials*, 37, 1821–1837. <https://doi.org/10.1177/002199803035186>
- Harding, J., & Welsh, L. M. (1983). A tensile testing technique for fibre-reinforced composites at impact rates of strain. *Journal of Materials Science*, 18, 1810–1826. <https://doi.org/10.1007/BF00542078>
- Hayes, S. V., & Adams, D. F. (1982). Rate sensitive tensile impact properties of fully and partially loaded unidirectional composites. *Journal of Testing and Evaluation*, 10, 61–68. <https://doi.org/10.1520/jte10234j>
- Hsiao, H. M., & Daniel, I. M. (1998). Strain rate behavior of composite materials. *Composites Part B: Engineering*, 29, 521–533. [https://doi.org/10.1016/S1359-8368\(98\)00008-0](https://doi.org/10.1016/S1359-8368(98)00008-0)
- Jacob, G. C., Starbuck, J. M., Fellers, J. F., et al. (2004). Strain rate effects on the mechanical properties of polymer composite materials. *Journal of Applied Polymer Science*, 94, 296–301. <https://doi.org/10.1002/app.20901>
- Janeliukstis, R., & Chen, X. (2021). Review of digital image correlation application to large-scale composite structure testing. *Composite Structures*, 271, 114143. <https://doi.org/10.1016/j.compstruct.2021.114143>

- Kawata K, Hondo A, Hashimoto S, et al (1981) Dynamic behavior analysis of composite materials.
- Khan, S. U., Iqbal, K., Munir, A., & Kim, J. K. (2011). Quasi-static and impact fracture behaviors of CFRPs with nanoclay-filled epoxy matrix. *Composites Part A: Applied Science and Manufacturing*, 42, 253–264. <https://doi.org/10.1016/j.compositesa.2010.11.011>
- Kim, M., Park, T. Y., & Hong, S. (2021). Experimental determination of the plastic deformation and fracture behavior of polypropylene composites under various strain rates. *Polymer Testing*, 93, 107010. <https://doi.org/10.1016/j.polymertesting.2020.107010>
- Kornmann, X., Rees, M., Thomann, Y., et al. (2005). Epoxy-layered silicate nanocomposites as matrix in glass fibre-reinforced composites. *Composites Science and Technology*, 65, 2259–2268. <https://doi.org/10.1016/j.compscitech.2005.02.006>
- Kotal, M., & Bhowmick, A. K. (2015). Polymer nanocomposites from modified clays: Recent advances and challenges. *Progress in Polymer Science*, 51, 127–187.
- Lam, C. K., Cheung, H. Y., Lau, K. T., et al. (2005). Cluster size effect in hardness of nanoclay/epoxy composites. *Composites Part B: Engineering*, 36, 263–269. <https://doi.org/10.1016/j.compositesb.2004.09.006>
- Li, G., & Liu, D. (2015). Low strain rate testing based on drop weight impact tester. *Experimental Techniques*, 39, 30–35. <https://doi.org/10.1111/j.1747-1567.2012.00862.x>
- Lifshitz, J. M. (1976). Impact strength of angle ply fiber reinforced materials. *Journal of Composite Materials*, 10, 92–101. <https://doi.org/10.1177/002199837601000108>
- Lifshitz, J. M., & Rotem, A. (1972). Longitudinal tensile failure of unidirectional fibrous composites. *Journal of Materials Science*, 7, 861–869. <https://doi.org/10.1007/BF00550433>
- Lin, L.-Y., Lee, J.-H., Hong, C.-E., et al. (2006). Preparation and characterization of layered silicate/glass fiber/epoxy hybrid nanocomposites via vacuum-assisted resin transfer molding (VARTM). *Composites Science and Technology*, 66, 2116–2125. <https://doi.org/10.1016/j.compscitech.2005.12.025>
- Liu, W., Hoa, S. V., & Pugh, M. (2005). Organoclay-modified high performance epoxy nanocomposites. *Composites Science and Technology*, 65, 307–316. <https://doi.org/10.1016/j.compscitech.2004.07.012>
- Majzoobi, G. H., Barton, D C, & Ramezani, M. (2007). Stress wave effects in the flying edge high strain rate tensile testing device. *The Journal of Strain Analysis for Engineering Design*, 42, 507–516. <https://doi.org/10.1243/03093247JSA289>
- Majzoobi, G. H., Saniee, F. F., & Bahrami, M. (2005). A tensile impact apparatus for characterization of fibrous composites at high strain rates. *Journal of Materials Processing Technology*, 162–163, 76–82. <https://doi.org/10.1016/j.jmatprotec.2005.02.182>
- Mohd Nurazzi, N., Asyraf, M. R. M., Khalina, A., et al. (2021). Fabrication, functionalization, and application of carbon nanotube-reinforced polymer composite: An overview. *Polymers*, 13, 1047. <https://doi.org/10.3390/polym13071047>
- Naresh, K., Shankar, K., Velmurugan, R., & Gupta, N. K. (2020). High strain rate studies for different laminate configurations of bi-directional glass/epoxy and carbon/epoxy composites using DIC. *Structure*, 27, 2451–2465. <https://doi.org/10.1016/j.istruc.2020.05.022>
- Nurazzi, N. M., Asyraf, M. R. M., Khalina, A., et al. (2021). A review on natural fiber reinforced polymer composite for bullet proof and ballistic applications. *Polymers*, 13, 646. <https://doi.org/10.3390/polym13040646>
- Ochola, R. O., Marcus, K., Nurick, G. N., & Franz, T. (2004). Mechanical behaviour of glass and carbon fibre reinforced composites at varying strain rates. *Composite Structures*, 63, 455–467. [https://doi.org/10.1016/S0263-8223\(03\)00194-6](https://doi.org/10.1016/S0263-8223(03)00194-6)
- Okoli, O. I. (2001). The effects of strain rate and failure modes on the failure energy of fibre reinforced composites. *Composite Structures*, 54, 299–303. [https://doi.org/10.1016/S0263-8223\(01\)00101-5](https://doi.org/10.1016/S0263-8223(01)00101-5)
- Okoli, O. I., & Smith, G. F. (2000). High strain rate characterization of a glass/epoxy composite. *Journal of Composites Technology and Research*, 22, 3–11. <https://doi.org/10.1520/ctr10619j>
- Omran, A. A. B., Mohammed, A. A. B. A., Sapuan, S. M., et al. (2021). Micro- and nanocellulose in polymer composite materials: A review. *Polymers*, 13, 231. <https://doi.org/10.3390/polym13020231>

- Pan, B. (2018). Digital image correlation for surface deformation measurement: Historical developments, recent advances and future goals. *Measurement Science and Technology*, 29, 082001. <https://doi.org/10.1088/1361-6501/aac55b>
- Pan, B., Qian, K., Xie, H., & Asundi, A. (2009). Two-dimensional digital image correlation for in-plane displacement and strain measurement: A review. *Measurement Science and Technology*, 20, 062001. <https://doi.org/10.1088/0957-0233/20/6/062001>
- Pardo, S., Baptiste, D., Décobert, F., et al. (2002). Tensile dynamic behaviour of a quasi-unidirectional E-glass/polyester composite. *Composites Science and Technology*, 62, 579–584. [https://doi.org/10.1016/S0266-3538\(01\)00152-X](https://doi.org/10.1016/S0266-3538(01)00152-X)
- Pavlidou, S., & Papaspyrides, C. D. (2008). A review on polymer-layered silicate nanocomposites. *Progress in Polymer Science (Oxford)*, 33, 1119–1198.
- Perogamvros, N., Mitropoulos, T., & Lampeas, G. (2016). Drop tower adaptation for medium strain rate tensile testing. *Experimental Mechanics*, 56, 419–436. <https://doi.org/10.1007/s11340-015-0112-3>
- Powell, L. A., Luecke, W. E., Merzkirch, M., et al. (2017). High strain rate mechanical characterization of carbon fiber reinforced polymer composites using digital image correlations. *SAE International Journal of Materials and Manufacturing*, 10, 138–146. <https://doi.org/10.4271/2017-01-0230>
- Qi, B., Zhang, Q. X., Bannister, M., & Mai, Y. W. (2006). Investigation of the mechanical properties of DGEBA-based epoxy resin with nanoclay additives. *Composite Structures*, 75, 514–519. <https://doi.org/10.1016/j.compstruct.2006.04.032>
- Quaresimin, M., & Varley, R. J. (2008). Understanding the effect of nano-modifier addition upon the properties of fibre reinforced laminates. *Composites Science and Technology*, 68, 718–726. <https://doi.org/10.1016/j.compscitech.2007.09.005>
- Raisch, S. R., & Möglinger, B. (2010). High rate tensile tests—Measuring equipment and evaluation. *Polymer Testing*, 29, 265–272. <https://doi.org/10.1016/j.polymertesting.2009.11.010>
- Ratna, D., Becker, O., Krishnamurthy, R., et al. (2003). Nanocomposites based on a combination of epoxy resin, hyperbranched epoxy and a layered silicate. *Polymer*, 44, 7449–7457. <https://doi.org/10.1016/j.polymer.2003.08.035>
- Roland, C. M., Twigg, J. N., Vu, Y., & Mott, P. H. (2007). High strain rate mechanical behavior of polyurea. *Polymer*, 48, 574–578. <https://doi.org/10.1016/j.polymer.2006.11.051>
- Sanusi, O. M., Benelfellah, A., & Aït Hocine, N. (2020). Clays and carbon nanotubes as hybrid nanofillers in thermoplastic-based nanocomposites—A review. *Applied Clay Science*, 185, 105408.
- Shadlou, S., Ahmadi-Moghadam, B., & Taheri, F. (2014). The effect of strain-rate on the tensile and compressive behavior of graphene reinforced epoxy/nanocomposites. *Materials & Designing*, 59, 439–447. <https://doi.org/10.1016/j.matdes.2014.03.020>
- Shi, Y., Kanny, K., & Jawahar, P. (2009). Hybrid Nanocomposites: Processing and Properties. *Advanced Composite Materials*, 18, 365–379. <https://doi.org/10.1163/156855109X434757>
- Shokrieh, M. M., & Omid, M. J. (2009). Tension behavior of unidirectional glass/epoxy composites under different strain rates. *Composite Structures*, 88, 595–601. <https://doi.org/10.1016/j.compstruct.2008.06.012>
- Staab, G. H., & Gilat, A. (1995). High strain rate response of angle-ply glass/epoxy laminates. *Journal of Composite Materials*, 29, 1308–1320. <https://doi.org/10.1177/002199839502901003>
- Suriani, M. J., Rapi, H. Z., Ilyas, R. A., et al. (2021). Delamination and manufacturing defects in natural fiber-reinforced hybrid composite: A review. *Polymers*, 13, 1323. <https://doi.org/10.3390/polym13081323>
- Tjong, S. C. (2006). Structural and mechanical properties of polymer nanocomposites. *Materials Science and Engineering R: Reports*, 53, 73–197.
- Velmurugan, R., & Mohan, T. P. (2004). Room temperature processing of epoxy-clay nanocomposites. *Journal of Materials Science*, 9, 7333–7339.
- Wang, L., Wang, K., Chen, L., et al. (2006). Preparation, morphology and thermal/mechanical properties of epoxy/nanoclay composite. *Composites Part A: Applied Science and Manufacturing*, 37, 1890–1896. <https://doi.org/10.1016/j.compositesa.2005.12.020>

- Welsh, L. M., & Harding, J. (1985). *Dynamic tensile response of unidirectionally-reinforced carbon epoxy and glass epoxy composites* (pp. 1517–1531). Metallurgical Soc Inc.
- Weng, F., Fang, Y., Ren, M., et al. (2021). Effect of high strain rate on shear properties of carbon fiber reinforced composites. *Composites Science and Technology*, 203. <https://doi.org/10.1016/j.compscitech.2020.108599>
- Wu, C. L., Zhang, M. Q., Rong, M. Z., & Friedrich, K. (2002). Tensile performance improvement of low nanoparticles filled-polypropylene composites. *Composites Science and Technology*, 62, 1327–1340. [https://doi.org/10.1016/S0266-3538\(02\)00079-9](https://doi.org/10.1016/S0266-3538(02)00079-9)
- Xiao, X. (2008). Dynamic tensile testing of plastic materials. *Polymer Testing*, 27, 164–178. <https://doi.org/10.1016/j.polymertesting.2007.09.010>
- Yasmin, A., Abot, J. L., & Daniel, I. M. (2003). Processing of clay/epoxy nanocomposites by shear mixing. *Scripta Materialia*, 49, 81–86. [https://doi.org/10.1016/S1359-6462\(03\)00173-8](https://doi.org/10.1016/S1359-6462(03)00173-8)
- Yasmin, A., Luo, J. J., Abot, J. L., & Daniel, I. M. (2006). Mechanical and thermal behavior of clay/epoxy nanocomposites. *Composites Science and Technology*, 66, 2415–2422. <https://doi.org/10.1016/j.compscitech.2006.03.011>
- Zainuddin, S., Hosur, M. V., Zhou, Y., et al. (2010). Experimental and numerical investigations on flexural and thermal properties of nanoclay–epoxy nanocomposites. *Materials Science and Engineering: A*, 527, 7920–7926. <https://doi.org/10.1016/j.msea.2010.08.078>
- Zebarjad, S. M., & Sajjadi, S. A. (2008). On the strain rate sensitivity of HDPE/CaCO<sub>3</sub> nanocomposites. *Materials Science and Engineering A*, 475, 365–367. <https://doi.org/10.1016/j.msea.2007.05.008>
- Zhou, Y., Pervin, F., Biswas, M. A., et al. (2006). Fabrication and characterization of montmorillonite clay-filled SC-15 epoxy. *Materials Letters*, 60, 869–873. <https://doi.org/10.1016/j.matlet.2005.10.042>